INTERNATIONAL JOURNAL FOR NUMERICAL METHODS IN FLUIDS, VOL. 18, 1021–1060 (1994)

THE INFLUENCE OF NORMAL FLOW BOUNDARY CONDITIONS ON SPURIOUS MODES IN FINITE ELEMENT SOLUTIONS TO THE SHALLOW WATER EQUATIONS

J. J. WESTERINK

Department of Civil Engineering and Geological Sciences, University of Notre Dame, Notre Dame, IN 46556, U.S.A.

R. A. LUETTICH JR.

Institute of Marine Sciences, University of North Carolina at Chapel Hill, 3431 Arendell Street, Morehead City, NC 28557, U.S.A.

J. K. WU

Mechanics Department, Huazhong University of Science and Technology, Wuhan, Hubei, People's Republic of China

AND

R. L. KOLAR

Department of Civil Engineering and Geological Sciences, University of Notre Dame, Notre Dame, IN 46556, U.S.A.

SUMMARY

Finite element solutions of the primitive equation (PE) form of the shallow water equations are notorious for the severe spurious $2\Delta x$ modes which appear. Wave equation (WE) solutions do not exhibit these numerical modes. In this paper we show that the severe spurious modes in PE solutions are strongly influenced by essential normal flow boundary conditions in the coupled continuity–momentum system of equations. This is demonstrated through numerical examples that avoid the use of essential normal flow boundary conditions either by specifying elevation values over the entire boundary or by implementing natural flow boundary conditions in the weak weighted residual form of the continuity equation. Results from a series of convergence tests show that PE solutions are of nearly the same quality as WE solutions when spurious modes are suppressed by alternative specification of the boundary conditions. Network intercomparisons indicate that varying nodal support does not excite spurious modes in a solution, although it does enhance the spurious modes introduced when an essential normal flow boundary condition is used.

Dispersion analysis of discrete equations for interior and boundary nodes offers an explanation of the observed solution behaviour. For certain PE algorithms a mixed situation can arise where the boundary nodes exhibit a monotonic (noise-free) dispersion relationship and the interior nodes exhibit a folded (noisy) dispersion relationship. We have found that the mixed situation occurs when all boundary nodes are specified elevation nodes (which are enforced as essential conditions in the continuity equation) or when specified flow boundary nodes are treated as natural boundary conditions in the continuity equation. In either case the effect is to generate a solution that is essentially free of noise. Apparently, the monotonic dispersion behaviour at the boundaries suppresses the otherwise noisy behaviour caused by the folded dispersion relation on the interior.

KEY WORDS Finite elements Shallow water equations Boundary conditions Dispersion analysis Spurious modes Wave equation Primitive equations

CCC 0271–2091/94/111021–40

Received 19 March 1990
Revised 3 September 1993

INTRODUCTION

Early finite element solutions to the shallow water equations are well known for the severe numerical oscillations that arise as a result of the spatial discretization. The earliest finite element schemes used the shallow water equations in their unmodified or primitive form and typically applied equal-order interpolating functions for both surface elevation and velocities.[1–4] Regardless of the type of element and order of Lagrange interpolation, these primitive equation (PE) equal-order interpolation schemes led to solutions with severe spurious oscillation modes in both sea surface elevation and velocities. These undesirable modes were often eliminated by applying some type of broadband dissipation scheme implemented by using artificially high eddy viscosity values,[5,6] averaging nodal solutions at intermediate locations[1,7] or using an inherently dissipative temporal discretization scheme.[4] The heavy-handed addition of artificial damping is generally recognized as highly undesirable since it changes the dynamics of the original set of continuum conservation statements.[8–12]

Based on their success in eliminating spurious pressure modes in finite element solutions to the Navier–Stokes equations, mixed interpolation schemes were extensively applied in the second generation of finite element solutions to the shallow water equations. The most successful mixed-order algorithms use either six-node quadratic triangles for velocities and three-node linear triangles for elevation or nine-node biquadratic quadrilaterals for velocity and four-node bilinear quadrilaterals for elevation.[13,14] These algorithms result in smooth solutions for surface elevation but severe oscillations are still prevalent in the velocity solution.[14,15]

Successful finite element solutions finally emerged when the continuum equations themselves were rearranged prior to applying any spatial discretization procedure. The most successful of these were based on the wave equation (WE) form of the shallow water equations. The WE formulation combines the momentum and continuity equations into a wave-type equation in elevation and solves this equation in conjunction with the primitive form of the momentum equations.[16,17] Extensive numerical tests and applications have demonstrated that WE formulations with equal-order interpolating functions for sea surface elevation and velocities produce very accurate solutions which are almost free of spurious modes.[14–28] A variety of derivative formulations which result in equations equivalent to the WE equation for surface elevation alone have also proven very successful.[29,30]

The origin of the severe spurious modes in finite-element-based solutions to the shallow water equations has been the topic of extensive analysis for quite some time.[13,16,30–33] We note that although non-linear cascading processes contribute to energy building up on the grid scale, the most severe $2\Delta x$ oscillations are a linear phenomenon and appear in the solutions of the entirely linearized shallow water equations. In PE schemes the spurious modes have been related to a folded dispersion relationship with allows multiple wave numbers to exist for a single forcing frequency.[30] Mixed interpolation PE schemes also have folded dispersion relationships; however, since the minimum wavelength for sea surface elevation is $4\Delta x$, the pertinent dispersion relationship is not folded for elevation and no spurious elevation mode exists.[13,14] Wave equation solutions to the shallow water equations on the other hand exhibit a monotonic dispersion relationship over the entire wavelength range (from $2\Delta x$ to infinity) and therefore the spurious $2\Delta x$-mode does not appear in either sea surface elevation or velocity.[14,30]

Our study focuses on the influence of boundary conditions on spurious oscillations in PE and WE solutions to the harmonic linearized shallow water equations. It has been known for quite some time that over-constraining boundary conditions can introduce spurious modes into Navier–Stokes and convection–diffusion equation solutions. Examples include the specification of tangential velocity boundary conditions in the Navier–Stokes equations, which forces a

spurious pressure mode,[34,35] as well as the specification of essential outflow boundary conditions in both the Navier–Stokes and convection–diffusion equations, which introduces spurious modes.[8,36] Recently boundary conditions have become a topic of increasing interest for solutions to the shallow water equations as well.[37–40]

In this paper we examine both the PE and WE solutions subject to different boundary condition implementations. Initially we consider the standard PE and WE formulations which enforce specified elevation boundary conditions as essential conditions in the continuity or wave equation respectively and no-normal-flow boundary conditions as essential conditions in the momentum equation (An essential condition means that the corresponding discrete conservation equation is eliminated and replaced by the specified boundary value.) We also study the PE and WE solutions subject to elevation boundary conditions specified over the entire boundary. Finally we examine a PE formulation cast into a weak weighted residual formulation. In this last formulation essential specified elevation boundary conditions on the seaward boundary are combined with natural no-normal-flow conditions on land boundaries (computed by a boundary integral that arises during the development of the weak form). A series of numerical experiments and convergence tests applied to Lynch and Gray's[41] quarter-annulus test problem with quadratically varying bathymetry demonstrate that while the WE-based solutions are insensitive to the implementation of the boundary conditions, i.e. the solutions are highly accurate and free of noise, the PE solutions are quite sensitive to the implementation of the boundary conditions. In particular, PE solutions that enforce no-normal-flow boundary conditions as essential conditions result in noisy solutions. Conversely, PE solutions that specify essential elevation boundary conditions on the entire boundary or that implement a natural no-normal-flow boundary condition within the framework of a weak weighted residual formulation give solutions that are free of numerical noise.

Dispersion analysis of the discrete equation pairs solved at interior and boundary nodes seems to offer an explanation for the observed solution behaviour. It is shown that whereas WE-based solutions always have monotonic dispersion curves at both interior and boundary nodes regardless of the boundary condition implementation, the dispersion behaviour of PE-based solutions can vary depending on the boundary conditions specified. Specifically, PE interior nodes as well as PE essential no-normal-flow boundary nodes have folded dispersion curves, while PE essential specified elevation boundary nodes and PE natural no-normal-flow boundary nodes have monotonic dispersion curves. To our knowledge a dispersion analysis of different boundary condition implementations and their correlation with numerical experiments has not been reported in the literature. Such an analysis appears to be a valuable tool in assessing the overall behaviour of the solution algorithm.

GOVERNING EQUATIONS

We examine the linearized form of the shallow water equations which are expressed as

$$\partial\zeta/\partial t + \nabla\cdot(h\mathbf{u}) = 0, \tag{1}$$

$$\partial(h\mathbf{u})/\partial t + gh\nabla\zeta + \mathbf{f}\times h\mathbf{u} + \tau_* h\mathbf{u} = 0, \tag{2}$$

where t is the time, ζ is the surface elevation relative to undisturbed sea level, $\mathbf{u}$ is the depth-averaged velocity vector, h is the depth of undisturbed sea level (bathymetry), g is the acceleration due to gravity, τ_* is the linearized bottom friction coefficient and $\mathbf{f}$ is the Coriolis parameter. We note that the conservative form of the momentum equation has been used.

Typically, boundary conditions are prescribed either with surface elevation ζ^* or normal flux Q_n^* which can be expressed as

$$\zeta(\mathbf{x}, t) = \zeta^*(\mathbf{x}, t) \quad \text{on } \Gamma_\zeta, \tag{3a}$$

$$Q_n(\mathbf{x}, t) = Q_n^*(\mathbf{x}, t) \quad \text{on } \Gamma_Q. \tag{3b}$$

For linearized equations the normal flux is computed as

$$Q_n = h\mathbf{u} \cdot \mathbf{n}, \tag{4}$$

where $\mathbf{n}$ is the unit outward normal vector to the boundary.

When boundary conditions and/or other forcings are entirely periodic, responses for the linearized shallow water equations are also periodic and of the form

$$\zeta(\mathbf{x}, t) = \mathrm{Re}[\hat{\zeta}(\mathbf{x})e^{\hat{\imath}\omega t}], \tag{5a}$$

$$\mathbf{u}(\mathbf{x}, t) = \mathrm{Re}[\hat{\mathbf{u}}(\mathbf{x})e^{\hat{\imath}\omega t}], \tag{5b}$$

where $\hat{\zeta}$ is the complex amplitude of the elevation, $\hat{\mathbf{u}}$ is the complex amplitude of the velocity vector, $\hat{\imath} = \sqrt{(-1)}$ and ω is the temporal frequency. This allows equations (1)–(3) to be simplified to the harmonic form

$$\hat{\imath}\omega\hat{\zeta} + \nabla \cdot (h\hat{\mathbf{u}}) = 0, \tag{6}$$

$$(\hat{\imath}\omega + \tau_*)h\hat{\mathbf{u}} + gh\nabla\hat{\zeta} + \mathbf{f} \times h\hat{\mathbf{u}} = 0, \tag{7}$$

$$\hat{\zeta}(\mathbf{x}) = \hat{\zeta}^*(\mathbf{x}) \quad \text{on } \Gamma_\zeta, \tag{8a}$$

$$\hat{Q}_n(\mathbf{x}) = \hat{Q}_n^*(\mathbf{x}) \quad \text{on } \Gamma_Q. \tag{8b}$$

Equations (1), (2) or (6), (7) are the basis for primitive equation (PE) formulations.

Equations (1) and (2) can be combined to form a wave equation (WE) which replaces the continuity equation in WE formulations.[16] The linear form of the WE is

$$\partial^2\zeta/\partial t^2 + \tau_* \, \partial\zeta/\partial t - h\mathbf{u} \cdot \nabla\tau_* - \nabla \cdot (gh\nabla\zeta + \mathbf{f} \times h\mathbf{u}) = 0. \tag{9}$$

In harmonic form the WE may be expressed as

$$\hat{\imath}\omega(\hat{\imath}\omega + \tau_*)\hat{\zeta} - h\hat{\mathbf{u}} \cdot \nabla\tau_* - \nabla \cdot (gh\nabla\hat{\zeta} + \mathbf{f} \times h\hat{\mathbf{u}}) = 0. \tag{10}$$

We note that equation (10) has been derived directly from the linearized time-dependent WE (9) and differs slightly from the spectral WE given by other investigators.[15,18,29] Their wave equation includes elevation as the only dependent variable and is therefore decoupled from the momentum equation. However, for cases without Coriolis forcing and a homogeneous friction factor τ_*, equation (10) is equivalent to that used by previous investigators. Finally we note that the same boundary conditions are usually applied for WE formulations as for PE formulations.

SOLUTIONS TO THE HARMONIC SHALLOW WATER EQUATIONS

The harmonic form of the linearized shallow water equations is investigated. In terms of accuracy the harmonic linearized shallow water equations for tidal problems have no associated time truncation errors or numerical problems related to the specification of the initial conditions.[10] Thus numerical inaccuracies arise purely from the spatial discretization.

Table I. Summary of various solution strategies used in solving the harmonic shallow water equations

Solution acronym	Formulation	Boundary conditions	Seaward boundary	Land boundary
PE-S	Primitive equation	Standard	Essential elevation	Essential no normal flow
WE-S	Wave equation	Standard	Essential elevation	Essential no normal flow in momentum and natural no normal flow in WE
PE-E	Primitive equation	Elevation	Essential elevation	Essential elevation
WE-E	Wave equation	Elevation	Essential elevation	Essential elevation
PE-W	Primitive equation	Weak	Essential elevation	Natural no normal flow

We examine and compare solutions using the PE formulation and WE formulation with boundary conditions implemented in various ways. Linear triangles are used to interpolate both elevations and velocities and fully consistent matrices are computed in all solutions. Seaward boundaries are always specified using surface elevations. The treatment of land boundary conditions includes the standard procedure for which normal flow boundary conditions are treated as essential conditions, the specification of elevation values over land boundaries and weak procedures where specified flow boundary conditions are treated as natural conditions. All the solutions presented in this section are summarized in Table I. Acronyms for each solution are also listed.

In order to evaluate each solution's performance and level of spurious oscillations, we solve Lynch and Gray's[41] popular quarter-annulus test problem with quadratically varying bathymetry. This stringent test problem poses potential numerical difficulties owing to its two-dimensional nature in addition to its variable bathymetry. The geometry consists of a quarter-annulus enclosed with land boundaries on three sides and a seaward boundary on the outer edge as shown in Figure 1. The dimensions used are an inner radius of $r_1 = 2 \times 10^5$ ft and an outer radius $r_2 = 5 \times 10^5$ ft. Bathymetry varies quadratically between $h = 10$ ft at r_1 and $h = 62{\cdot}5$ ft ar r_2. The linear bottom friction coefficient is specified as $\tau_* = 0{\cdot}0001\ \mathrm{s}^{-1}$ and the Coriolis parameter is set to zero. A tidal forcing period of 12·4 h is applied at the seaward boundary. The grid used in the computations is the irregular triangular network shown in Figure 2. This particular patched network presents possible numerical difficulties owing to the highly variable nodal support which alternates between four and eight nodes.

Primitive equation formulation with standard boundary conditions (PE-S)

We first consider the solution of the primitive equations using standard conditions (PE-S). Thus essential elevation boundary conditions are implemented on the seaward boundary and essential no-normal-flow boundary conditions are implemented on the land boundary.

The Galerkin weighted residual statements for the harmonic continuity equation (6) and momentum equation (7) are respectively

$$\mathrm{i}\omega\langle\hat{\zeta}, \phi_i\rangle + \langle\nabla\cdot(h\hat{\mathbf{u}}), \phi_i\rangle = 0, \tag{11}$$

$$\langle(\mathrm{i}\omega + \tau_*)h\hat{\mathbf{u}}, \phi_i\rangle + g\langle h\nabla\hat{\zeta}, \phi_i\rangle + \langle\mathbf{f}\times h\hat{\mathbf{u}}, \phi_i\rangle = 0, \tag{12}$$

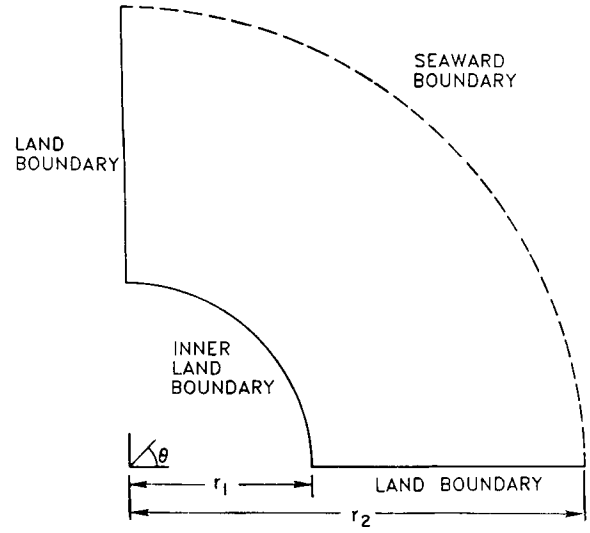

Figure 1. Geometry and boundaries for the quarter-annulus test problem

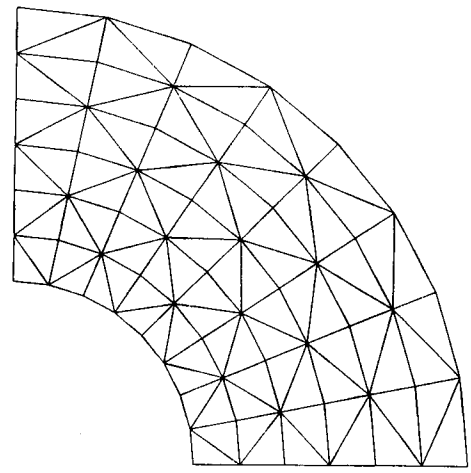

Figure 2. Irregular triangular grid at an intermediate level of refinement

where $\langle f_1, f_2 \rangle \equiv \int_\Omega f_1 f_2 \, d\Omega$ and ϕ_i are the interpolating basis functions. The use of C^0 linear interpolating bases to represent both elevation and velocity and exact integration techniques leads to the following global system of algebraic equations for the continuity and momentum equations:

$$\mathbf{M_C}\hat{\zeta} + \mathbf{D_C}\hat{\mathbf{U}} = 0, \tag{13}$$

$$\mathbf{M_M}\hat{\mathbf{U}} + \mathbf{D_M}\hat{\zeta} = 0, \tag{14}$$

where $\hat{\zeta}$ is the nodal elevation vector, $\hat{\mathbf{U}}$ is the nodal velocity vector, $\mathbf{M_C}$ and $\mathbf{D_C}$ are the

continuity equation coefficient matrices and $\mathbf{M}_M$ and $\mathbf{D}_M$ are the momentum equation coefficient matrices.

Both elevation and normal flow boundary conditions are treated as essential boundary conditions. Therefore continuity equations in system (13) corresponding to boundary nodes with specified sea surface elevations are eliminated and replaced by the specified nodal sea surface boundary condition value. Equation pairs in (14) corresponding to land boundary nodes with specified normal flow boundary equations are first reoriented in a normal/tangential co-ordinate system. The reoriented equations which correspond to the specified normal flow directions are then eliminated and replaced by the specified nodal normal flow boundary condition value.[5,42] The systems of equations (13) and (14) are solved simultaneously.

For the quarter-annulus test problem, elevation values on the entire seaward boundary are specified as $\hat{\zeta}^* = 0{\cdot}1$ ft and normal flow values on the entire land boundary are specified as zero. The PE-S solution is compared with Lynch and Gray's[41] analytical solution in Figure 3. Both the cosine and sine components of the elevation and radial velocity solutions are shown. The cosine and sine components are respectively defined as the coefficients of $\cos(\omega t)$ and $\sin(\omega t)$ in the solution expression. The predicted numerical solution at any value of θ is contained between the maximum and minimum nodal values plotted. Owing to symmetry and the fact that the Coriolis parameter is set to zero, the exact solution is the same for all θ.

The PE-S solution exhibits the severe spurious modes for which PE solutions are well known. Oscillations occur in both the radial and angular directions. The cosine component of elevation and corresponding sine component of radial velocity exhibit the worst oscillations. We note that this solution is almost identical to that published by Lynch.[18] Small differences exist since we are using the conservative form of the momentum equations.

Wave equation formulation with standard boundary conditions (WE-S)

We next consider the wave equation solution to the shallow water equations using standard boundary conditions (WE-S). Seaward boundary conditions are again specified with $\hat{\zeta}^* = 0{\cdot}1$ ft and are implemented as essential boundary conditions in the WE. Land boundary conditions are specified as no-normal-flow conditions and are now implemented as natural boundary conditions in the WE and essential boundary conditions in the momentum equations.

The Galerkin weak weighted residual statement for the WE is readily developed using (10) and the steps described by Lynch and Gray:[16]

$$\langle(-\omega^2 + \hat{\imath}\omega\tau_*)\hat{\zeta}, \phi_i\rangle + \langle(gh\nabla\hat{\zeta} + h\mathbf{f} \times \hat{\mathbf{u}}), \nabla\phi_i\rangle - \langle h\hat{\mathbf{u}}\nabla\tau_*, \phi_i\rangle = -\int_{\Gamma_Q} (\hat{\imath}\omega + \tau_*)\hat{Q}_n\phi_i \, d\Gamma. \tag{15}$$

Again C^0 linear bases are used to represent both elevations and velocities and exact numerical integration is used to yield the following global system of algebraic equations for the WE:

$$\mathbf{M}_W\hat{\boldsymbol{\zeta}} + \mathbf{D}_W\hat{\mathbf{U}} = \hat{\mathbf{P}}_W, \tag{16}$$

where $\mathbf{M}_W$ and $\mathbf{D}_W$ are the wave equation coefficient matrices and $\hat{\mathbf{P}}_W$ is the load vector for prescribed normal flow boundaries.

The WE (16) considers boundary condition information on both prescribed normal flow boundaries, which are included in the boundary integral term represented by $\hat{\mathbf{P}}_W$, and prescribed elevation boundaries, which are included through the nodal boundary equation substitution procedure described previously. The discretization and handling of boundary conditions for the

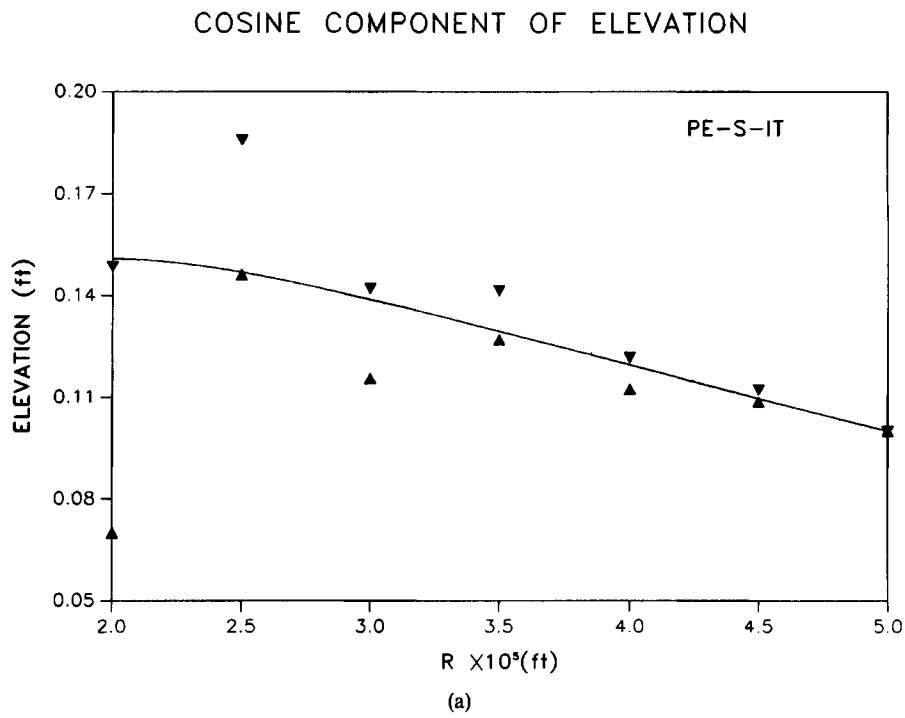

Figure 3. Harmonic primitive equation solution with standard boundary conditions (PE-S)

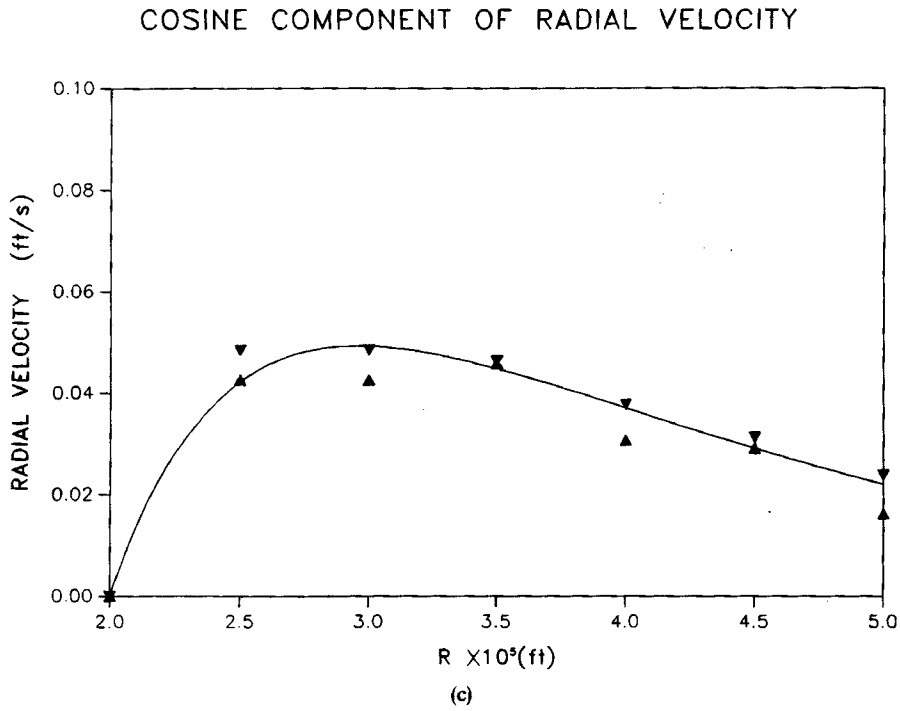

(c)

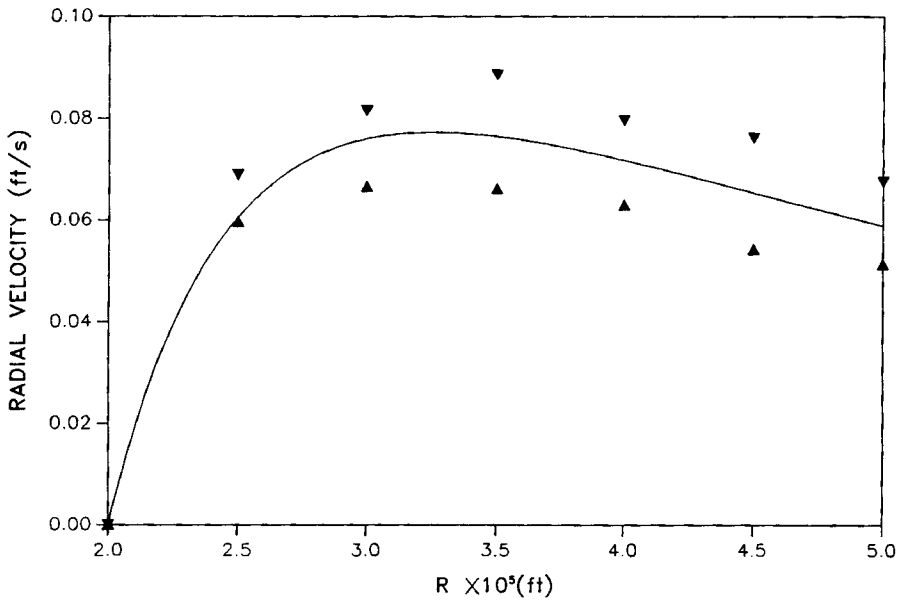

(d)

Figure 3. (*Continued*)

momentum equation are exactly the same as for the PE-S formulation described in the previous subsection. Thus the WE formulation also solves (14) after the inclusion of prescribed normal flow boundary conditions as essential boundary conditions. The coupled system of equations formed by (16) and (14) is solved simultaneously.

The WE-S solution for the quarter-annulus test problem with the same boundary conditions as for the PE-S solution is shown in Figure 4. The results are excellent and exhibit essentially no spurious modes. Some components of the solution do appear to be slightly damped. We note that this solution almost coincides with previously published WE solutions to this problem.[18] Very slight differences exist owing to the fact that we are using the conservative form of the momentum equations.

Primitive equation and wave equation formulations with entirely specified elevation boundary conditions (PE-E and WE-E)

We now examine the behaviour of the PE and WE solutions described in the previous subsections when surface elevation boundary conditions are specified over both the seaward and land boundaries in the quarter-annulus test problem (PE-E and WE-E solutions). Thus elevation values on the seaward boundary are prescribed as $\hat{\zeta}^* = 0{\cdot}1$ ft and elevation values on the land boundaries are prescribed using Lynch and Gray's[41] analytical solution. Normal flow boundary conditions are not included in the solution; hence their influence can be conveniently assessed in intermodel comparisons.

The PE-E solution to the test problem is shown in Figure 5 and the WE-E solution is shown in Figure 6. It is remarkable to note that the PE-E and WE-E solutions with prescribed elevation boundary conditions over the entire domain are very similar. There are essentially no spurious oscillations in either elevation solution, although the PE-E velocity solution is slightly noisier than the WE-E velocity solution. Both velocity solutions exhibit a loss of accuracy near the inner land boundary since no boundary constraints are imposed on the velocity solution.

The entirely specified elevation boundary condition solutions presented in this subsection indicate that the interior domain discretization strategies of the PE and WE can lead to very similar solutions. Furthermore, the experiment clearly demonstrates that boundary conditions can fundamentally affect the solution. In fact, it appears that the treatment of no-normal-flow boundary conditions as essential conditions significantly influences the generation of spurious modes in PE solutions.

Primitive equation formulation with weak normal flow boundary conditions (PE-W)

Results from the previous subsection demonstrate the detrimental influence of essential no-normal-flow boundary conditions in the momentum equations on the quality of PE solutions. We now develop a PE solution in which normal flow boundary conditions are treated as natural boundary conditions in the continuity equation and are not implemented in the momentum equations (PE-W solution). Prescribed elevation boundary conditions are treated as essential conditions as was done in the PE-S scheme.

A weak weighted residual form for the continuity equation is readily established by intergrating the second term in equation (11) by parts, which leads to

$$\hat{\imath}\omega\langle\hat{\zeta}, \phi_i\rangle - \langle h\hat{\mathbf{u}}, \nabla\phi_i\rangle = -\int_{\Gamma_Q} h\hat{\mathbf{u}} \cdot \mathbf{n}\phi_i \, d\Gamma. \tag{17}$$

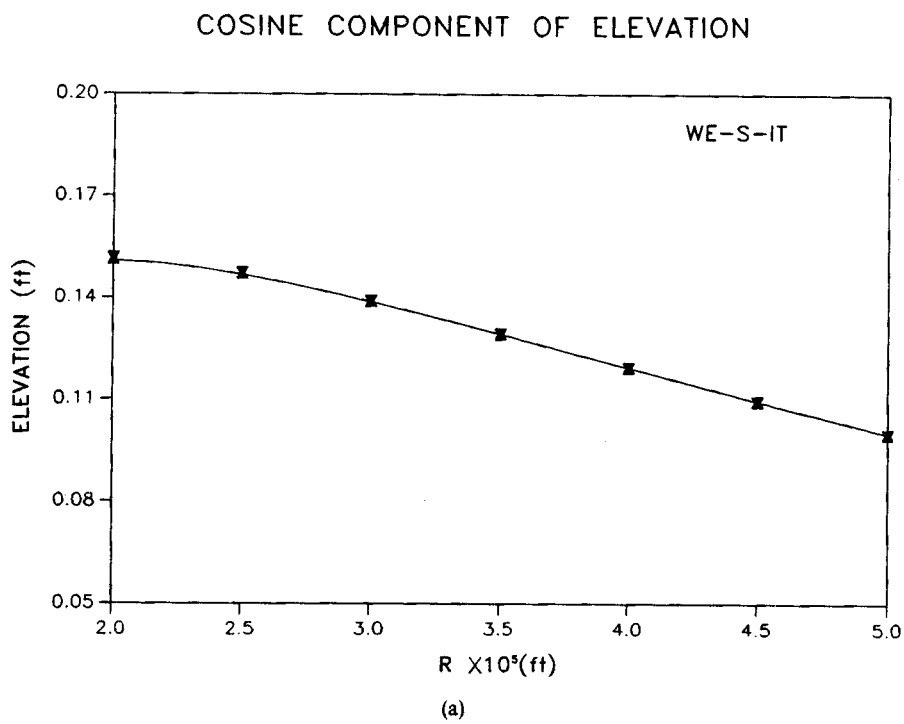

(a)

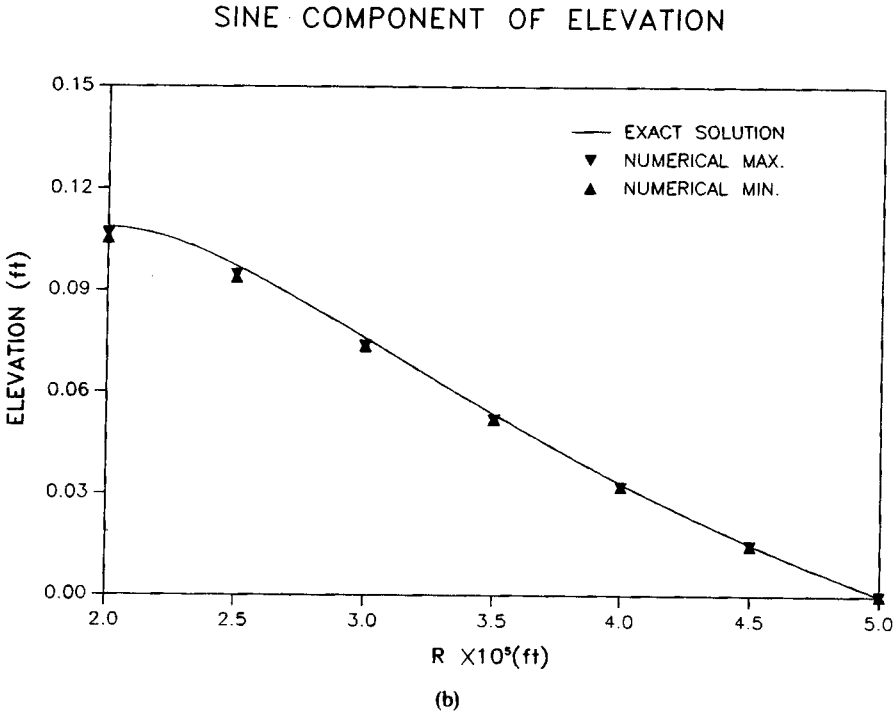

(b)

Figure 4. Harmonic wave equation solution with standard boundary conditions (WE-S)

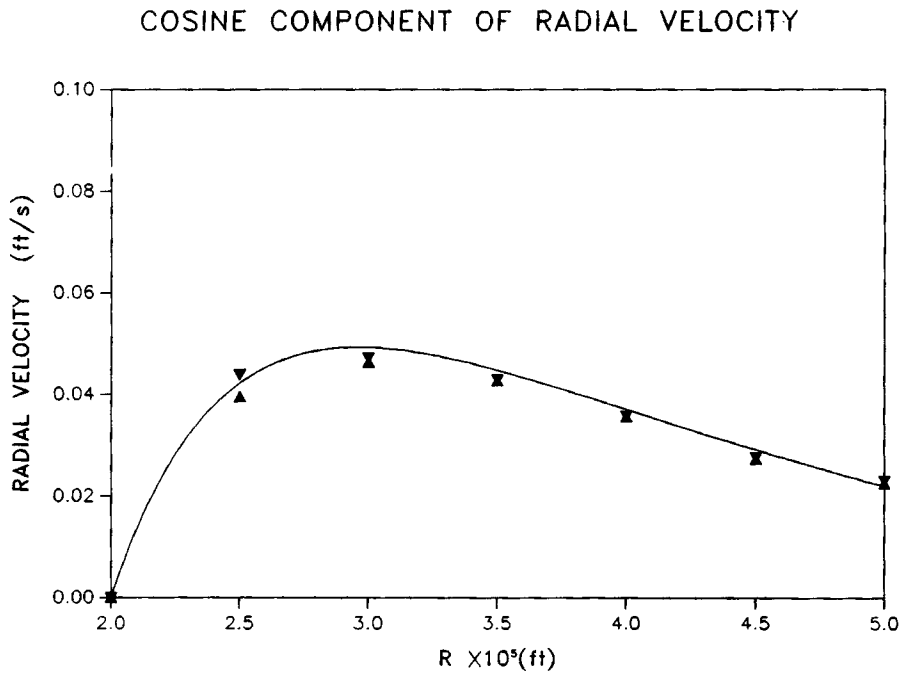

(c)

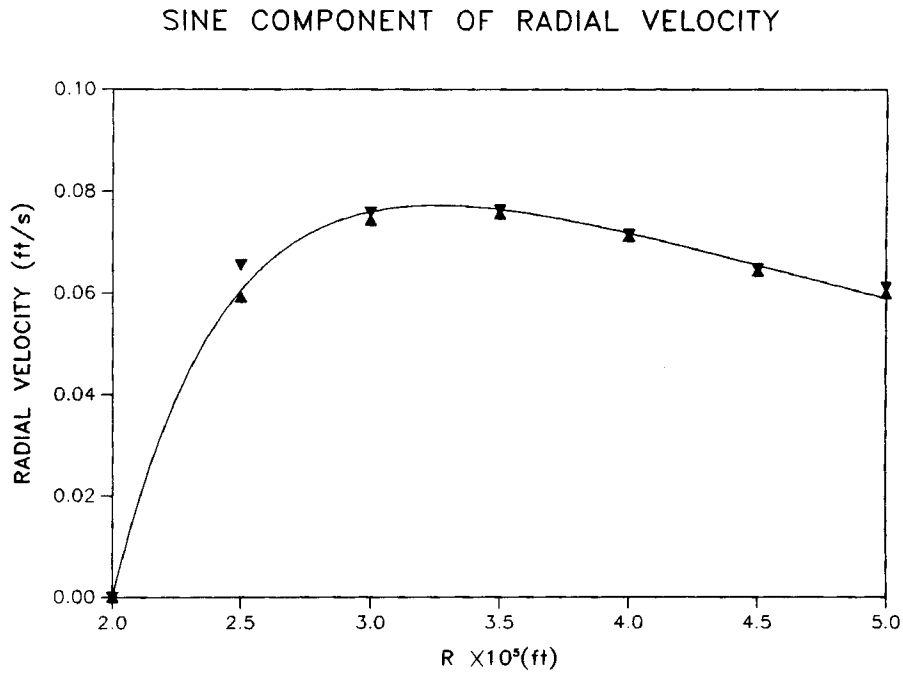

(d)

Figure 4. (*Continued*)

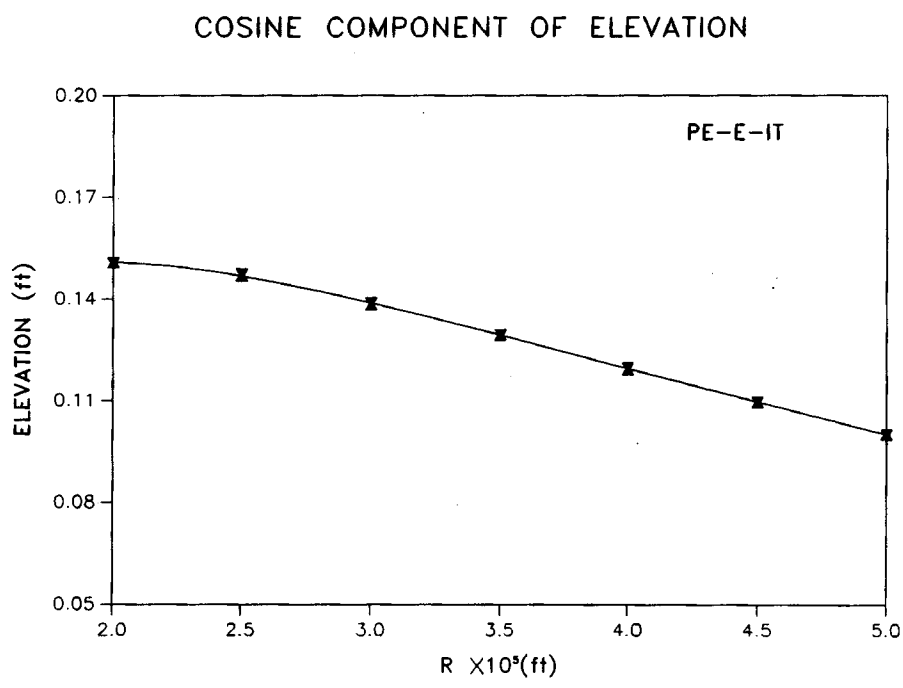

(a)

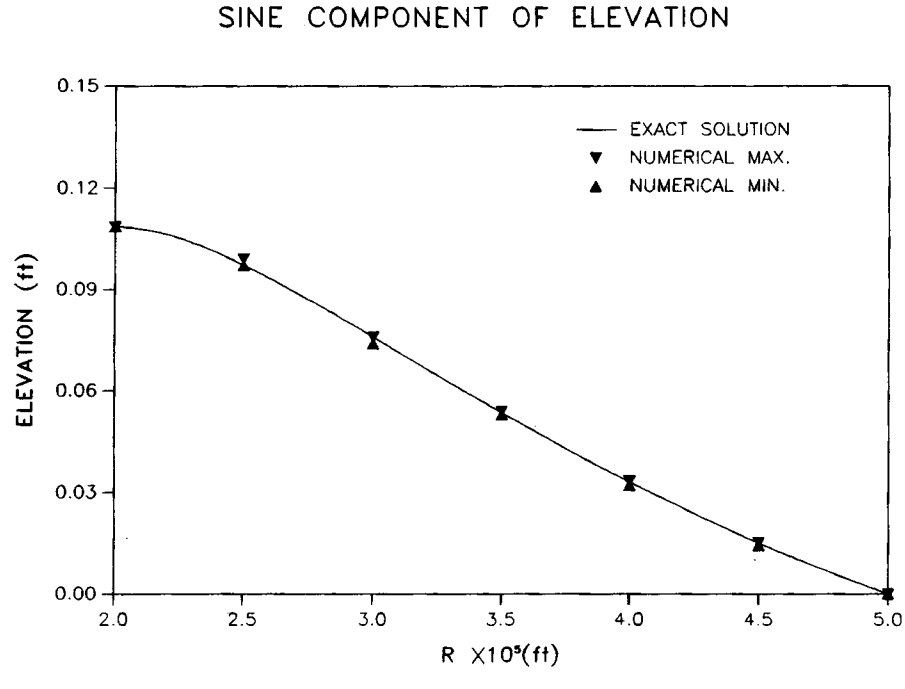

(b)

Figure 5. Harmonic primitive equation solution with elevation boundary conditions specified on the entire boundary (PE-E)

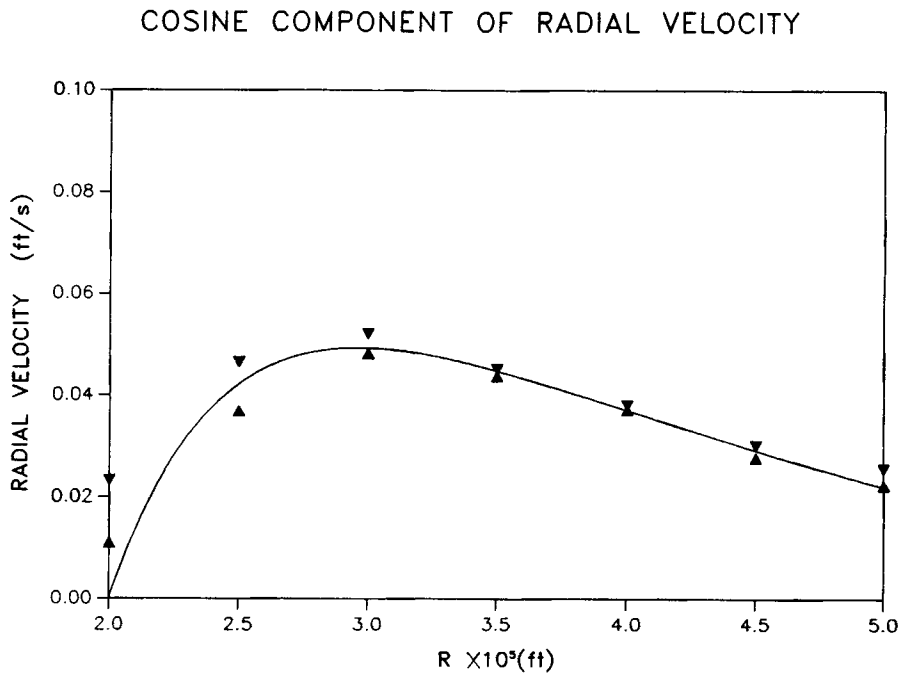

(c)

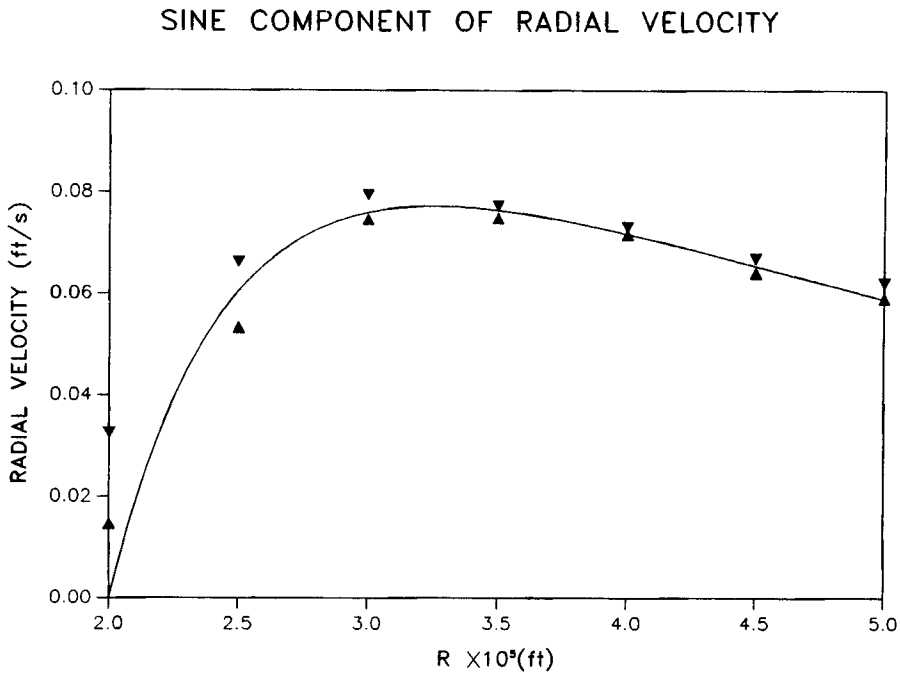

(d)

Figure 5. (*Continued*)

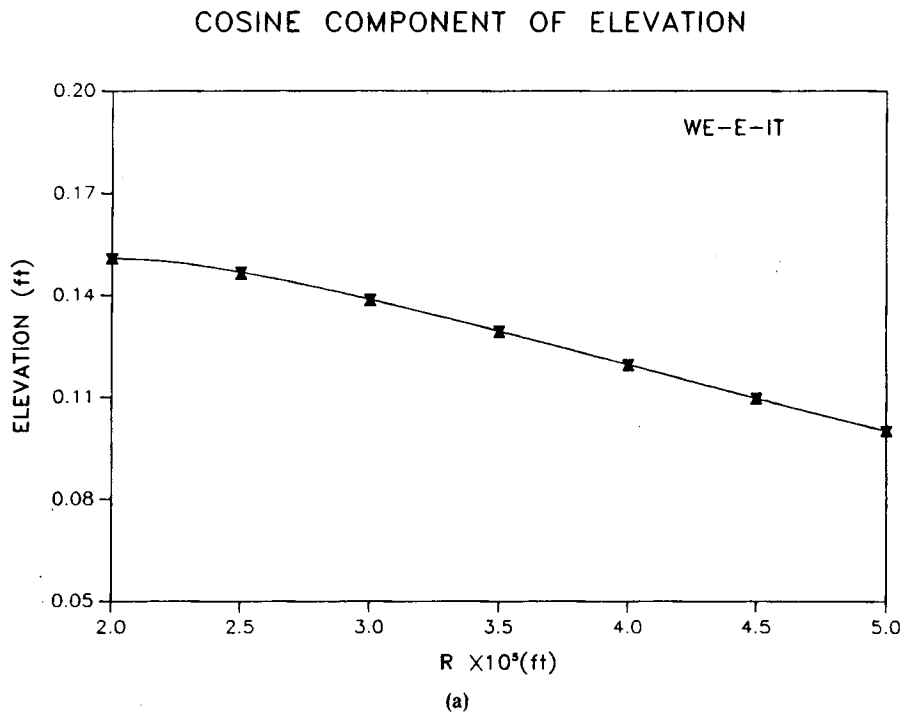

Figure 6. Harmonic wave equation solution with elevation boundary conditions specified on the entire boundary (WE-E)

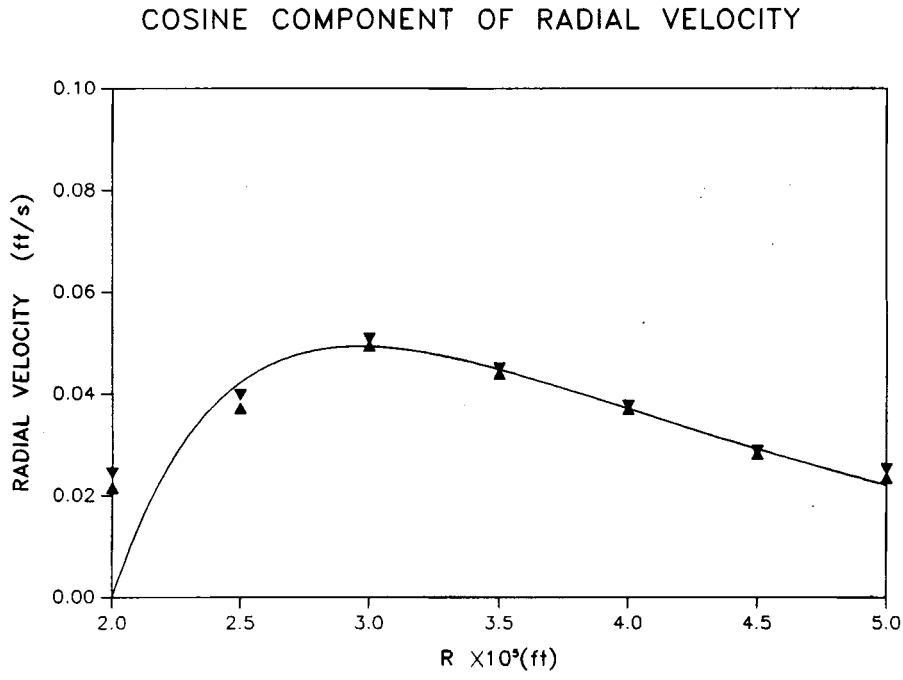

(c)

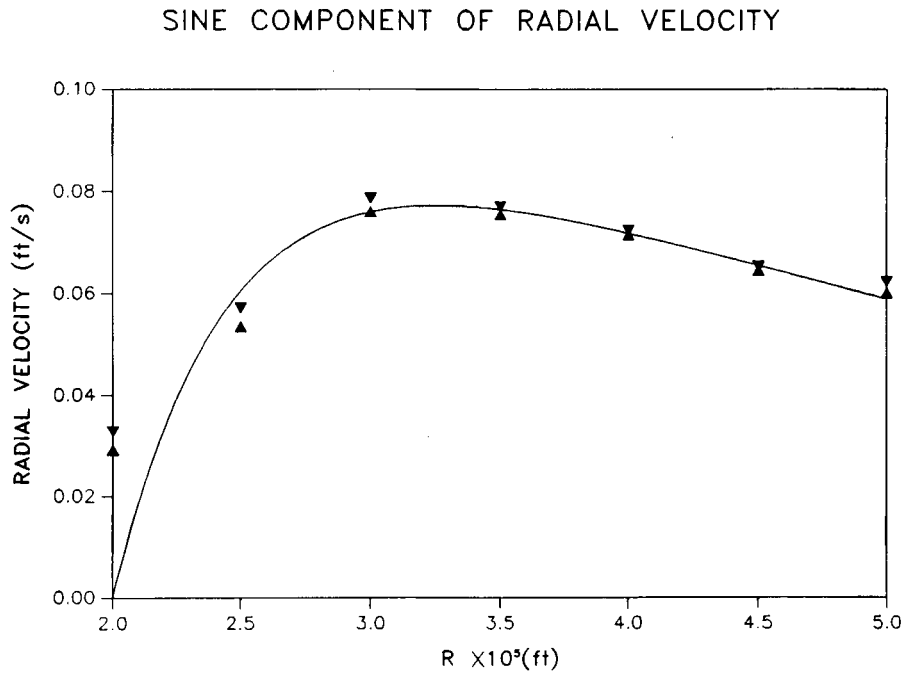

Figure 6. (*Continued*)

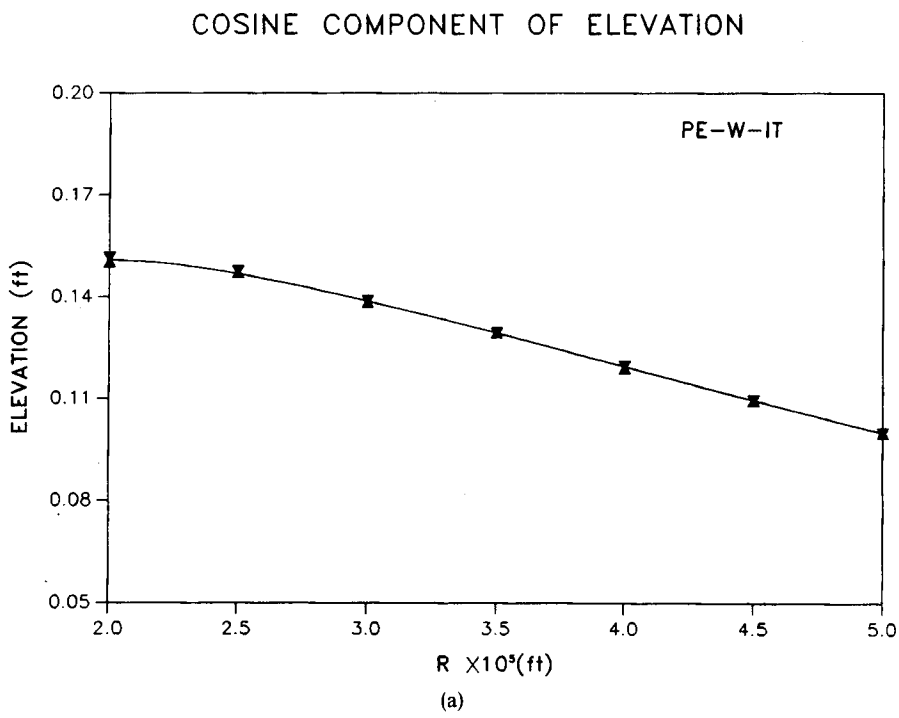

Figure 7. Harmonic primitive equation solution with weak normal flow boundary conditions (PE-W)

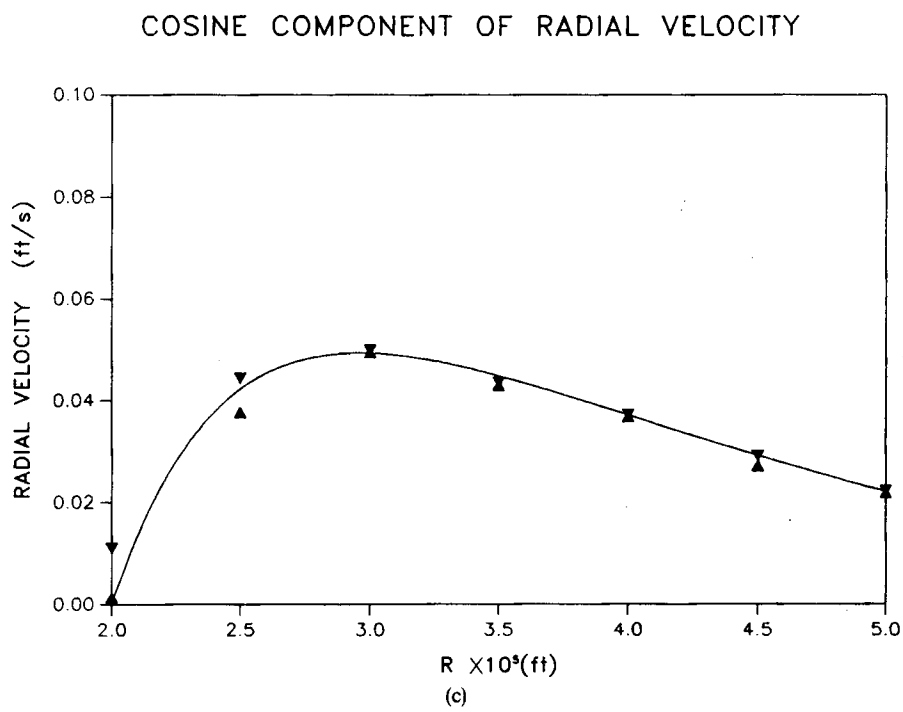

(c)

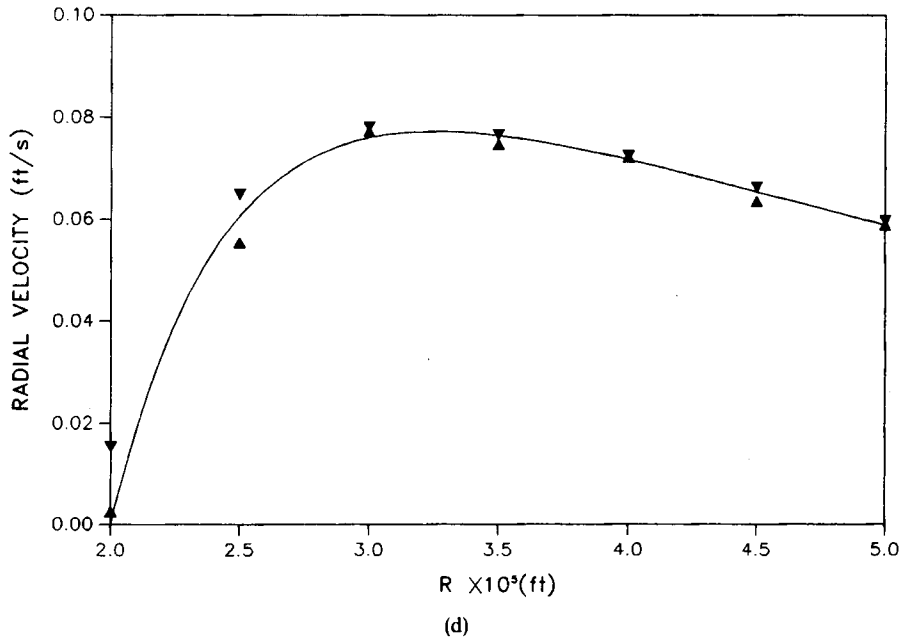

(d)

Figure 7. (*Continued*)

Integration using equal-order C^0 linear interpolants yields the following system of global equations for the PE-W formulation:

$$\mathbf{M}_{\text{C-W}}\hat{\boldsymbol{\zeta}} + \mathbf{D}_{\text{C-W}}\hat{\mathbf{U}} = \hat{\mathbf{P}}_{\text{C-W}}, \tag{18}$$

where $\mathbf{M}_{\text{C-W}}$ and $\mathbf{D}_{\text{C-W}}$ are the weak continuity equation coefficient matrices and $\hat{\mathbf{P}}_{\text{C-W}}$ is the load vector for prescribed normal flow boundaries.

Thus equation (18) includes information on prescribed normal flow boundaries, which is embedded in the surface integral term $\hat{\mathbf{P}}_{\text{C-W}}$, as well as prescribed elevation boundary conditions, which is included through the nodal boundary condition substitution procedure. The discretized momentum equations for the PE-W scheme are again represented by (14). However, normal flow boundary condition information is not incorporated into this set of momentum equations since it is already included in the continuity equation as a natural boundary condition. The systems of equations (18) and (14) with the boundary conditions implemented as described are solved simultaneously.

The PE-W solution to the quarter-annulus problem with the seaward boundary specified as $\hat{\zeta}^* = 0{\cdot}1$ ft and the land boundary specified as a natural no-normal-flow condition is shown in Figure 7. The severe spurious modes which typically appear in PE solutions are not present. The elevation solution is excellent and without almost any discernible oscillations. The velocity solution away from the inner boundary is in general also very good and exhibits only slight oscillations. At the inner boundary the velocity solution is relatively poor, as was the case for the PE-E and WE-E solutions, since no essential velocity constraints are imposed at the land boundary. We note that the PE-W solution is dramatically better than the PE-S solution (cf. Figure 3). In fact, the overall quality of the PE-W solution is similar to that of the WE-S solution (except for the velocity solution near the inner boundary). Although the oscillations are slightly larger than in the WE-S solution, the PE-W solution does not experience the slight damping seen in the WE-S solution.

The lack of severe spurious modes in the PE-W solution again illustrates that the spurious modes in PE solutions are strongly influenced by strictly enforcing normal flow conditions in the momentum equation as essential boundary conditions.

CONVERGENCE RATE STUDIES OF THE HARMONIC PE-S, WE-S AND PE-W SOLUTIONS FOR VARIOUS NETWORKS

In this section we present further comparisons of the harmonic PE-S, WE-S and PE-W schemes described previously. Specifically, we examine spatial convergence rates for various degrees of mesh refinement in addition to the effect of different networks.

Again the quarter-annulus quadratic bathymetry test problem serves as the basis of our comparison study. Seaward boundary conditions are specified as $\hat{\zeta}^* = 0{\cdot}1$ ft and land boundary conditions are prescribed with no-normal-flow conditions for all solutions. The degree of mesh refinement varies considerably and includes the very coarse 3×4 grid in Figure 8(a), the intermediate 6×8 grid used previously and presented in Figure 2, the fine 9×12 grid shown in Figure 8(b) and the very fine 12×16 grid shown in Figure 8(c). Element shape is maintained for all four grids. In addition to the four grids with linear triangles arranged in an irregular pattern with variable nodal support (four or eight), we also examined a corresponding sequence of regular linear triangular networks with a constant nodal support of six as well as bilinear quadrilateral networks. Sample networks for the two latter meshes are shown in Figures 9(a) and 9(b) respectively at an intermediate level of refinement.

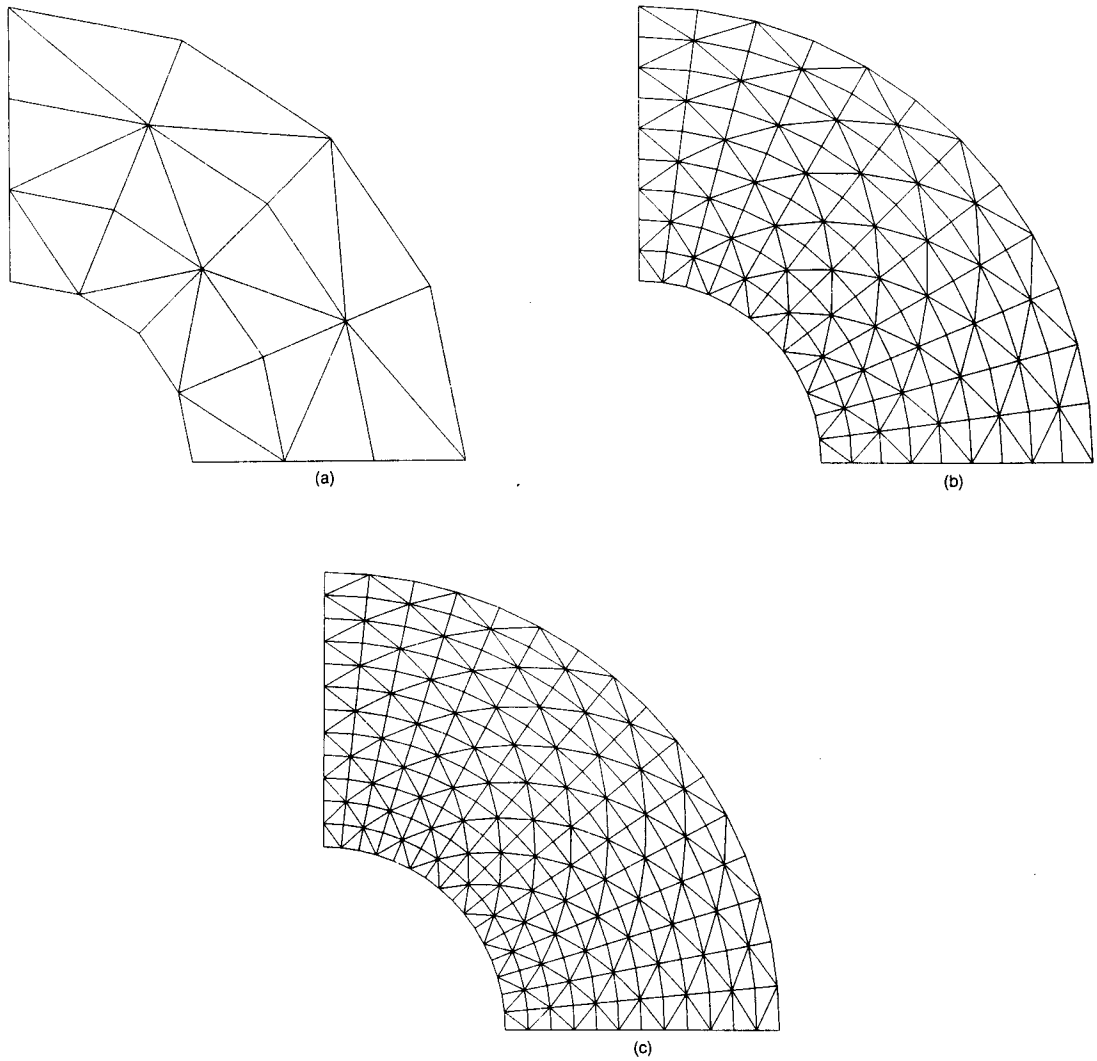

Figure 8. Irregular triangular grids (a) at a very coarse level of refinement, (b) at a fine level of refinement and (c) at a very fine level of refinement

In order to quantify the performance of each scheme and network, we compute a global L_2 norm, normalized with respect to the area of the domain, which may be defined as

$$E_{L_2} \equiv \left(\frac{1}{A} \int_{\Omega} (S_N - S_E)^2 \, dx \, dy \right)^{1/2} \tag{19}$$

where S_N represents the numerical cosine and sine components of the elevation and radial velocity solutions, S_E represents the corresponding components of the exact solution and A is the area of the domain Ω. The E_{L_2} norm represents an average global error for the components of the elevation and velocity solutions.

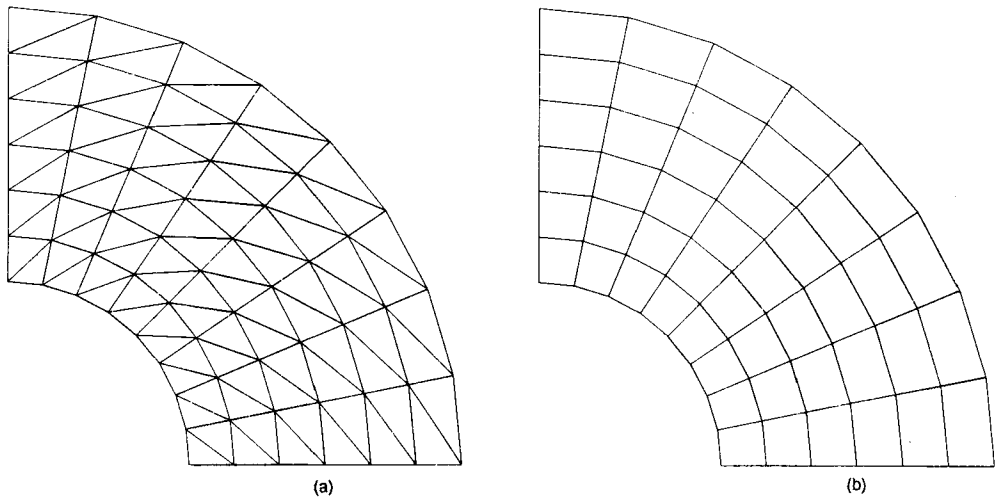

Figure 9. (a) Regular triangular grid at an intermediate level of refinement and (b) bilinear quadrilateral grid at an intermediate level of refinement

We first examine solutions to the sequence of irregular triangular (IT) networks. The L_2 error norm for the cosine and sine components of the elevation and velocity solutions are plotted against the radial discretization length in Figure 10 for all three schemes. It is clear that the PE-S-IT scheme fares the worst by far owing to the severe spurious modes associated with this scheme. Although the scheme does converge, serious spurious oscillations are still apparent even for the very finest level of discretization. The accuracy of the WE-S-IT scheme is in general excellent for both elevations and velocities, since essentially no spurious modes are present in these solutions. The PE-W-IT solutions are excellent in elevation, since suprious modes are not present when normal flow boundary conditions are not treated as essential conditions, but these solutions do still exhibit significant L_2 errors in velocity owing to the flow leakage problems at the inner boundary. The PE-W-IT convergence curve for the cosine component of elevation is essentially identical to that of the WE-S-IT solution. Furthermore, the convergence curve for the sine component of elevation is somewhat better than that of the WE-S-IT solution owing to the slight amount of damping which shows up in the WE-S solutions for this component. The PE-W-IT velocity solution is worse than the WE-S-IT solution owing to the PE-W scheme's inherent velocity errors at the inner land boundary.

The convergence characteristics (as measured by the L_2 error norm) for the sequence of regular triangular (RT) networks shown in Figure 11 are basically the same as for the IT networks. The PE-S-RT scheme is the only solution for which the convergence curves differ substantially from the corresponding IT solution. Although the cosine component of the PE-S-RT elevation solution is better than that of the PE-S-IT solution, the sine component of the elevation solution is worse. Furthermorre, the PE-S-RT cosine velocity component is substantially worse than the PE-S-IT solution, with much larger wiggles, whereas the sine velocity component is a little better. The convergence curves for the WE-S-RT and PE-W-RT solutions are almost identical to the corresponding IT solutions.

Finally, the convergence trends for the bilinear quadrilateral (Q) networks shown in Figure 12 are very similar to those for the RT and IT schemes. Again the PE-S-Q scheme is the only

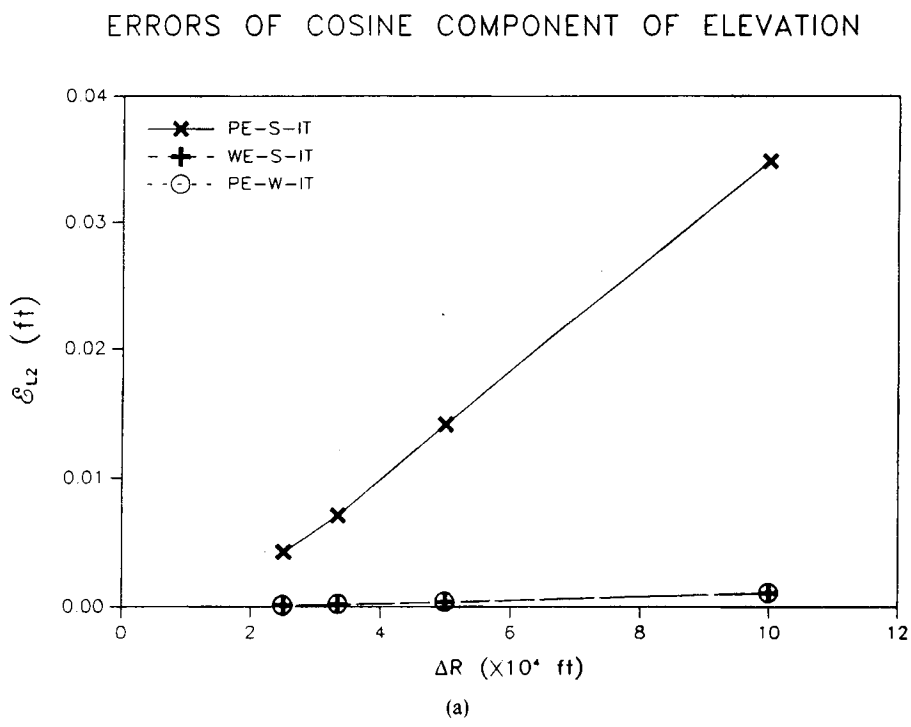

Figure 10. L_2 error norm spatial convergence curves for harmonic PE-S, WE-S and PE-W schemes for irregular triangular networks

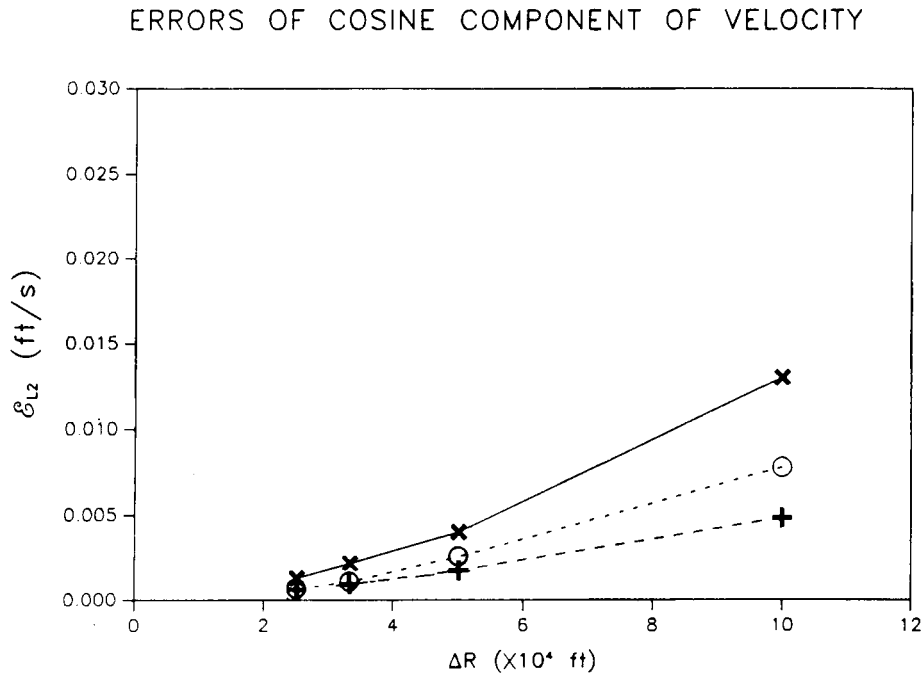

(c)

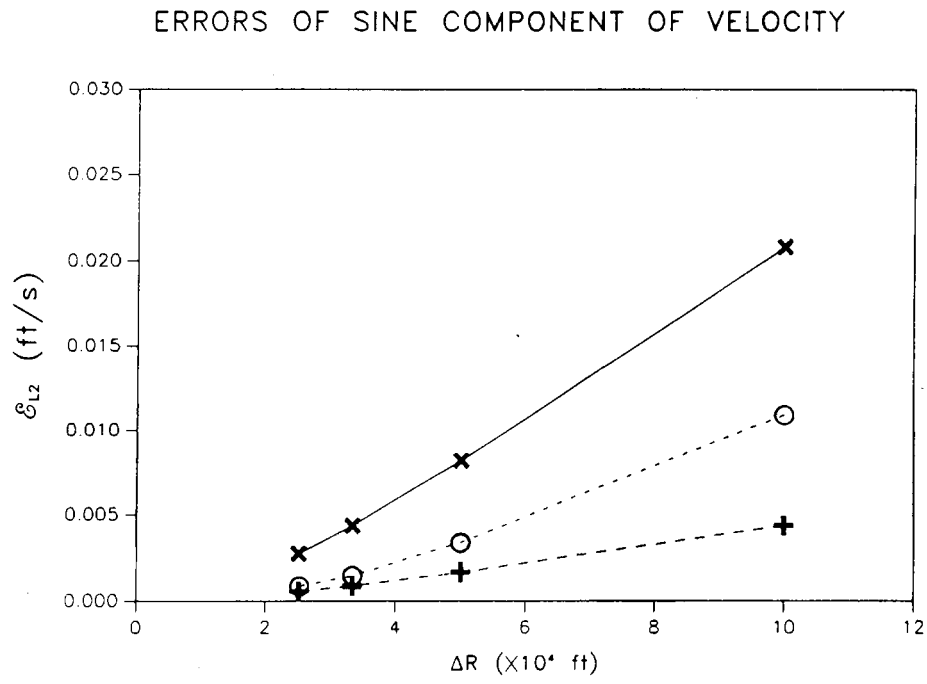

(d)

Figure 10. (*Continued*)

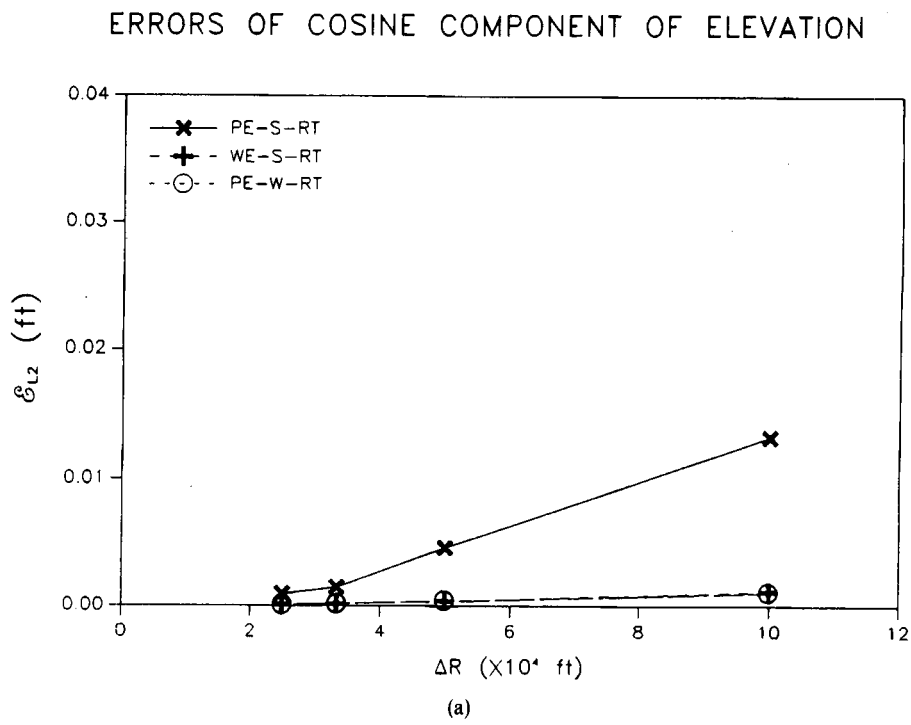

(a)

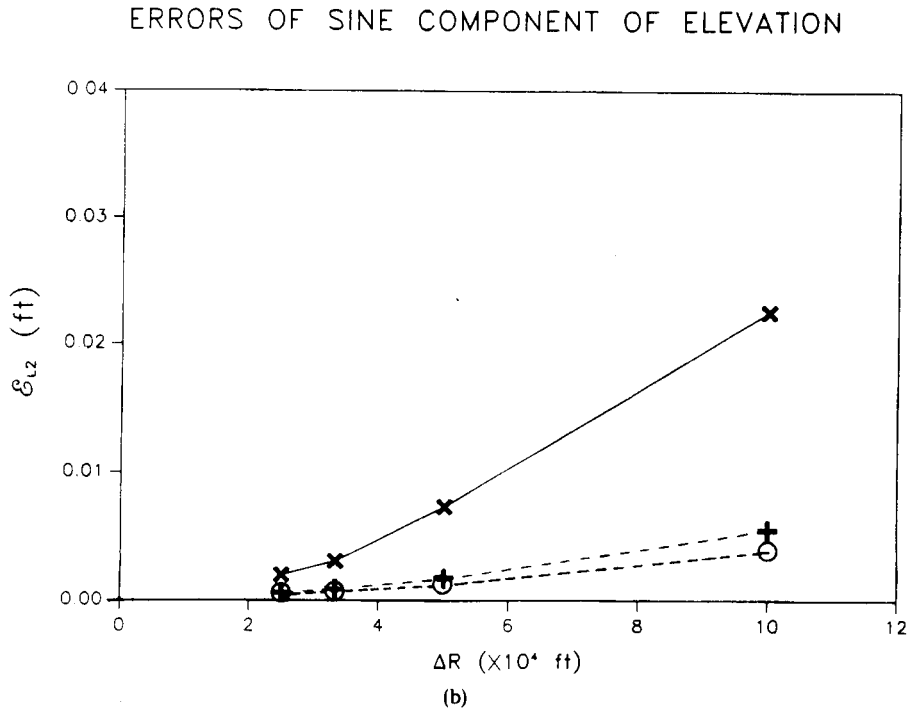

(b)

Figure 11. L_2 error norm spatial convergence curves for harmonic PE-S, WE-S and PE-W schemes for regular triangular networks

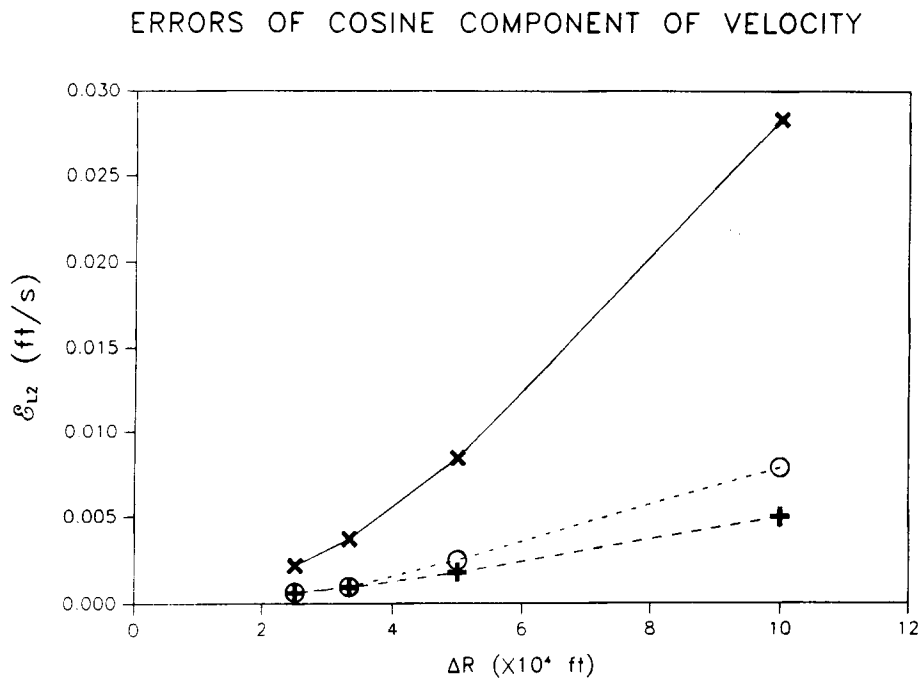

(c)

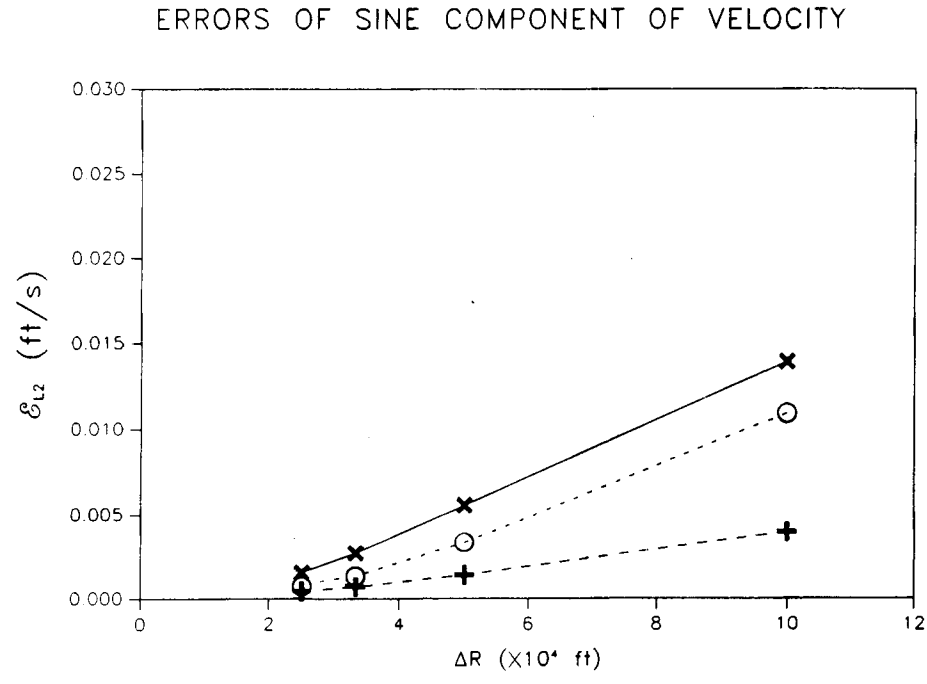

(d)

Figure 11. (*Continued*)

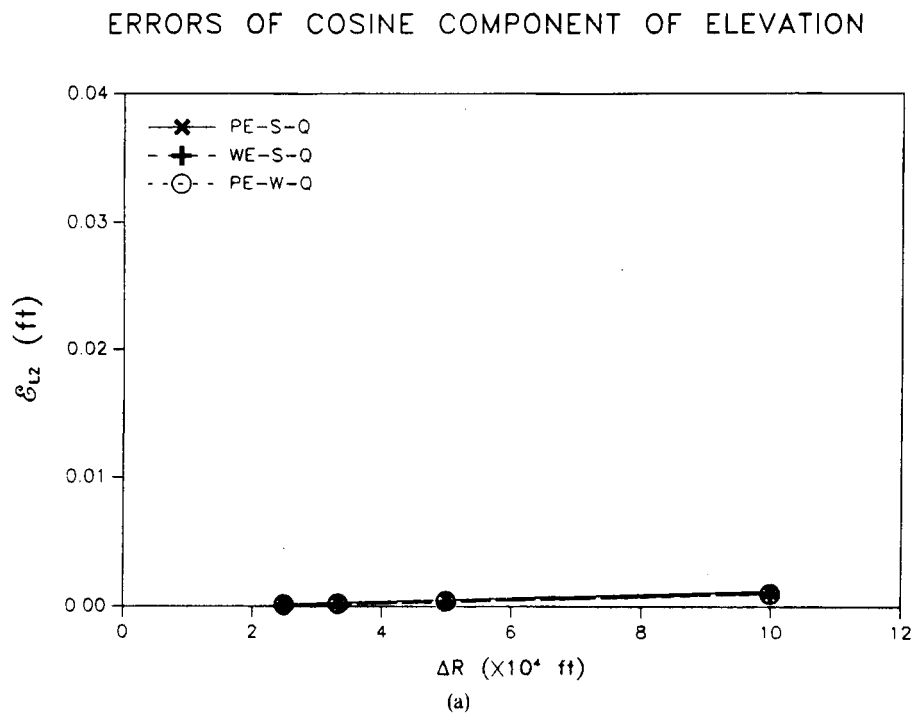

(a)

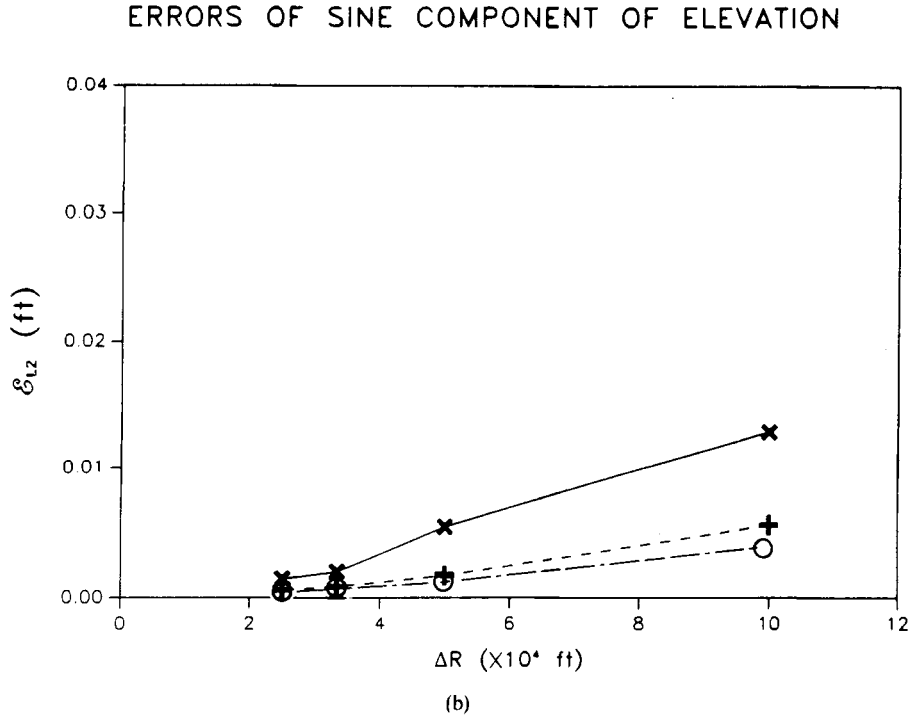

(b)

Figure 12. L_2 error norm spatial convergence curves for harmonic PE-S, WE-S and PE-W schemes for bilinear quadrilateral networks

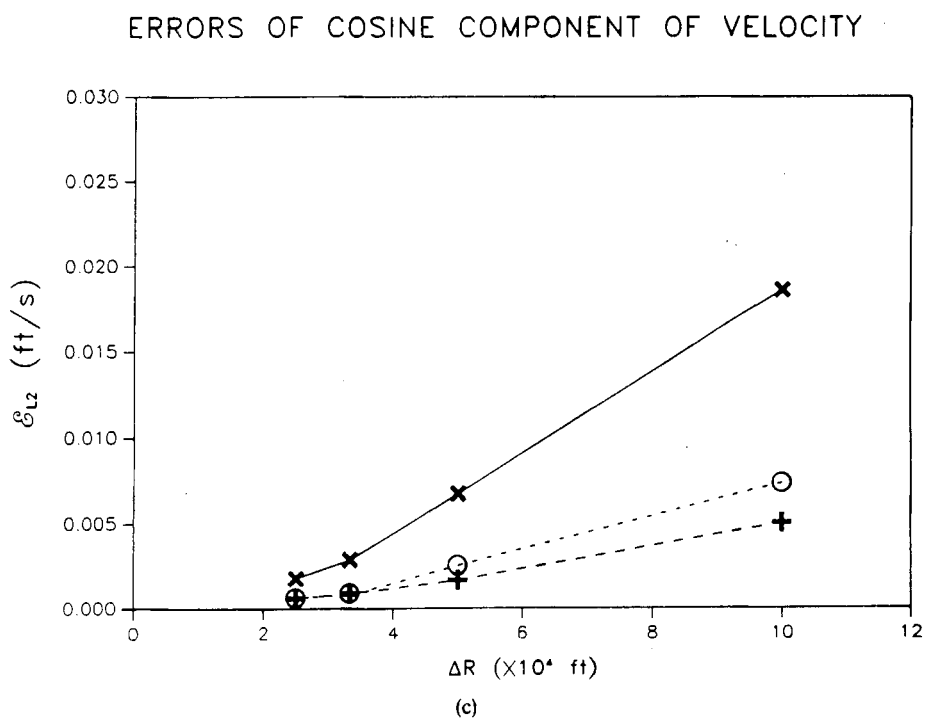

(c)

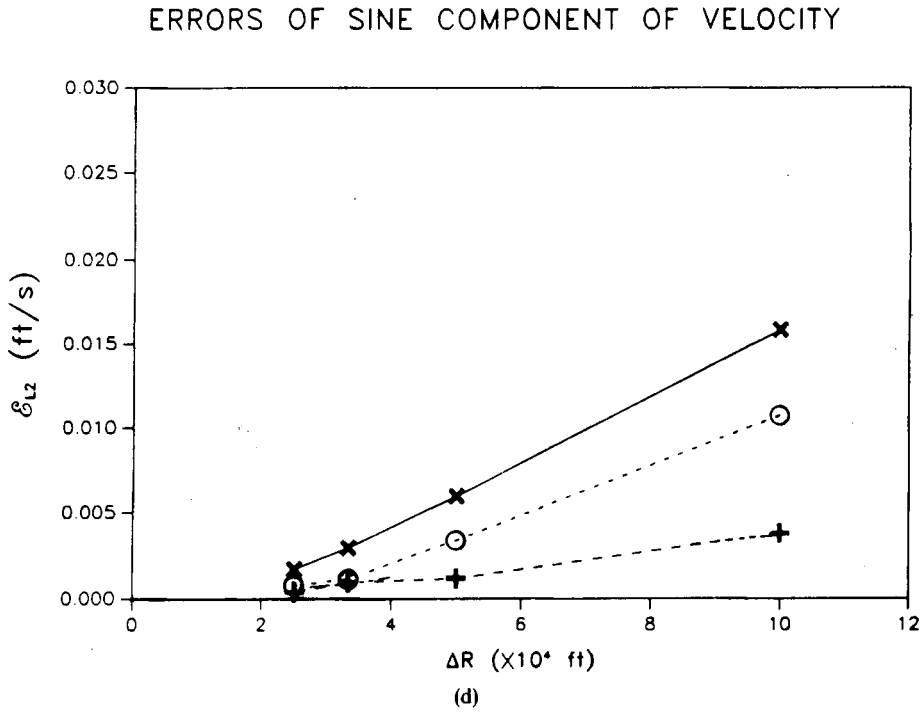

(d)

Figure 12. (*Continued*)

solution which differs significantly from the solution obtained with the triangular networks. In fact, the cosine component of the PE-S-Q elevation solution is now idential to the other schemes and does not exhibit spurious modes. Although the sine component of the PE-S-Q elevation solution does exhibit some spurious modes, the L_2 error norms are significantly better than for the IT and RT networks. However, the PE-S-Q velocity solutions have convergence curves which lie between those of the IT and RT solutions. The WE-S-Q and PE-W-Q schemes have almost identical convergence curves as for the IT and RT networks. We note that the PE-S-Q solution exhibits only radial oscillations and that no angular oscillations are present, whereas the PE-W-Q solution exhibits slight radial oscillations and very slight angular oscillations.

In summary, for all networks examined, the PE-S solution is clearly the worst owing to the presence of severe spurious $2\Delta x$ modes. We note that it is only when the spurious $2\Delta x$ modes are present (in the PE-S solution) that there appears to be a significant grid dependence on the quality of the solution.

DISPERSION ANALYSIS

In the numerical experiments and convergence tests presented in this paper, we note that the quality of WE-based solutions is relatively insensitive to the boundary conditions specified. However, PE-based solutions are significantly influenced by boundary condition implementation. In this section we apply dispersion analysis to study the propagation characteristics of the various discrete equation sets on the interior domain as well as on the boundary and we correlate the findings with results from the numerical experiments. Platzman[30] first applied dispersion analysis to the shallow water equations and was able to identify the fundamental difference between PE and WE discrete equations on interior nodes. He found that PE solutions on interior nodes have a folded dispersion curve which allows two wave numbers per frequency (one physical long wave and a second near-$2\Delta x$ non-physical short wave), whereas the WE-based solutions have a monotonic dispersion curve which allows only one wave number per frequency (the physical long wave). Note that a monotonic dispersion relation is also a characteristic of the continuum solution.

In order to study the sensitivity of PE and WE solutions to boundary condition implementation, we apply dispersion analysis to the discrete sets of equations associated with interior domain nodes as well as with boundary nodes. The cases examined are listed in Table II. These cases allow us to discern the behaviour of the various solutions considered in the numerical experiments. We note that the first two cases are well-known standard analysis[14,30,43] but are included for the sake of completeness. All analyses are based on discrete equations derived from the one-dimensional form of the linear harmonic shallow water equations, (6) and (7), and of the linear harmonic WE, (10). Assumptions of constant bathymetry and no Coriolis forcing are also made. In addition, linear finite elements are applied in all cases and fully consistent matrices are used.

Case 1. Primitive continuity and momentum equations on interior nodes

We first analyse the well-known PE solution on interior nodes. The discrete form of the primitive continuity and momentum equations applied to a generic interior node j for all PE-based solutions may be written as

$$(\hat{\imath}\omega/6)(\hat{\zeta}_{j-1} + 4\hat{\zeta}_j + \hat{\zeta}_{j+1}) + (h/2\Delta x)(\hat{u}_{j+1} - \hat{u}_{j-1}) = 0, \tag{20}$$

$$(\hat{\imath}\omega + \tau_*)(h/6)(\hat{u}_{j-1} + 4\hat{u}_j + \hat{u}_{j+1}) + (gh/2\Delta x)(\hat{\zeta}_{j+1} - \hat{\zeta}_{j-1}) = 0. \tag{21}$$

Table II. Summary of discrete equations on the interior and on the boundary to which dispersion analysis is applied

Case	Discrete continuity equation	Discrete momentum equation	Location
1	Primitive continuity	Momentum	Interior node
2	Wave equation	Momentum	Interior node
3	Primitive continuity	No-normal-flow boundary condition	Boundary node
4	Wave equation	No-normal flow boundary condition	Boundary node
5	Elevation boundary condition	Momentum	Boundary node
6	Primitive weak continuity including natural no-normal-flow boundary condition	Momentum	Boundary node

For linear systems we can examine the solution behaviour by analysing only one component of a complex Fourier series representation of the solution. Thus elevation and velocity are written respectively as one-component series in space

$$\hat{\zeta}_j = Z_0 e^{i\sigma x_j}, \tag{22}$$

$$\hat{u}_j = U_0 e^{i\sigma x_j}, \tag{23}$$

where σ is a generic wave number, Z_0 and U_0 represent the elevation and velocity amplitudes of the Fourier component being examined respectively and x_j is the spatial location of node j. Substituting for $\hat{\zeta}_j$ and $\hat{u}_j$ into equations (20) and (21), noting that $x_j \equiv j\Delta x$, simplifying and writing the resulting equations in matrix form, we obtain

$$\begin{bmatrix} (\hat{\imath}\omega/6)(4 + \Sigma + \Sigma^{-1}) & (h/2\Delta x)(\Sigma - \Sigma^{-1}) \\ (gh/2\Delta x)(\Sigma - \Sigma^{-1}) & (\hat{\imath}\omega + \tau_*)(h/6)(4 + \Sigma + \Sigma^{-1}) \end{bmatrix} \begin{bmatrix} z_0 \\ U_0 \end{bmatrix} = \begin{bmatrix} 0 \\ 0 \end{bmatrix}, \tag{24}$$

where

$$\Sigma \equiv e^{i\sigma\Delta x}. \tag{25}$$

The determinant of the matrix in (24) must be zero for a non-trivial solution to exist and therefore we must have

$$\omega^2 - \hat{\imath}\tau_*\omega + \frac{3^2(\Sigma - \Sigma^{-1})^2}{(4 + \Sigma + \Sigma^{-1})^2} \frac{gh}{\Delta x^2} = 0. \tag{26}$$

For convenience we define the dimensionless frequency, dimensionless wave number and dimensionless friction factor respectively

$$\Omega \equiv \omega\Delta x/\pi\sqrt{(gh)}, \tag{27}$$

$$K \equiv \sigma\Delta x/\pi, \tag{28}$$

$$T_* \equiv \tau_*/\sigma\sqrt{(gh)}. \tag{29}$$

Thus equation (26), which describes the necessary condition for a non-trivial solution, can be expressed using dimensionless variables as

$$\Omega^2 - \hat{\imath} T_* K \Omega + \left(\frac{3(\Sigma - \Sigma^{-1})}{\pi(4 + \Sigma + \Sigma^{-1})} \right)^2 = 0. \tag{30}$$

Solving for the roots of (30), we have

$$\Omega_{1,2}^{\text{case-1}} = \frac{\hat{\imath} T_* K}{2} \pm \left(-\frac{T_*^2 K^2}{4} - \frac{3^2(\Sigma - \Sigma^{-1})^2}{\pi^2(4 + \Sigma + \Sigma^{-1})^2} \right)^{1/2}. \tag{31}$$

Equation (31) represents the dispersion relationship for a PE solution at an interior node and relates frequency and wave number. Physically, $\Omega_{1,2}^{\text{case-1}}$ describe a progressive and a regressive wave respectively. These numerical roots are compared with the roots from the analytical solution to the continuum form of the shallow water equations; the analytical roots are given by

$$\Omega_{1,2}^{\text{exact}} = \frac{\hat{\imath} T_* K}{2} \pm \left(-\frac{T_*^2 K^2}{4} + K^2 \right)^{1/2}. \tag{32}$$

In Figure 13 the absolute values of the dimensionless frequencies for both Case 1 and the analytical solution are plotted against dimensionless wave number for a frictional case with $T_* = 0{\cdot}4$. We note from Figure 13 that whereas the analytical solution has a monotonic linear dispersion curve, the PE solution at an interior node has a folded dispersion curve, allowing two wave numbers for a wide frequency range. The low-wave-number solution corresponds to

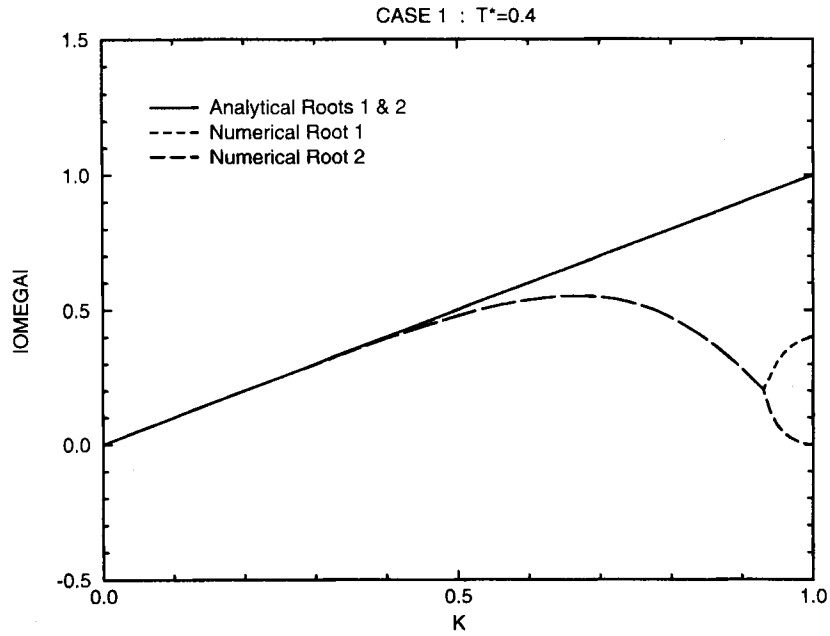

Figure 13. Dispersion curves for Case 1, primitive continuity and momentum equations on interior nodes

a long physical wave and the high-wave-number solution corresponds to a short near-$2\Delta x$ artificial wave ($K = 1{\cdot}0$ for a $2\Delta x$ wave). Platzman[30] first identified this folded dispersion curve as the origin of spurious modes in PE-based solutions to the shallow water equations. Finally we note the consistency of the PE solution in that as K approaches zero (i.e. for very long waves), the analytical and numerical dispersion curves converge.

Case 2. Wave equation and momentum equation on interior nodes

We now examine the WE solution on interior nodes. The discrete forms of the wave equation and momentum equation for all interior nodes for WE-based solutions are

$$-(\omega/6)(\omega - \hat{\imath}\tau_*)(\hat{\zeta}_{j-1} + 4\hat{\zeta}_j + \hat{\zeta}_{j+1}) + (gh/\Delta x^2)(-\hat{\zeta}_{j-1} + 2\hat{\zeta}_j - \hat{\zeta}_{j+1}) = 0, \tag{33}$$

$$(\hat{\imath}\omega + \tau_*)(h/6)(\hat{u}_{j-1} + 4\hat{u}_j + \hat{u}_{j+1}) + (gh/2\Delta x)(\hat{\zeta}_{j+1} - \hat{\zeta}_{j-1}) = 0. \tag{34}$$

Applying Fourier analysis by substituting (22) and (23) into (33) and (34) and simplifying the resulting equations leads to the following system of equations:

$$\begin{bmatrix} -(\omega/6)(\omega - \hat{\imath}\tau_*)(4 + \Sigma + \Sigma^{-1}) + (hg/\Delta x^2)(2 - \Sigma - \Sigma^{-1}) & 0 \\ (gh/2\Delta x)(\Sigma - \Sigma^{-1}) & (\hat{\imath}\omega + \tau_*)(h/6)(4 + \Sigma + \Sigma^{-1}) \end{bmatrix} \begin{bmatrix} Z_0 \\ U_0 \end{bmatrix} = \begin{bmatrix} 0 \\ 0 \end{bmatrix}. \tag{35}$$

Again for a non-trivial solution the matrix in (35) must have a determinant equal to zero. This determinant may be expressed using the dimensionless variables defined in (27)–(29) as

$$(\hat{\imath}\Omega + T_* K)\left(\Omega^2 - \hat{\imath}T_* K\Omega - \frac{6}{\pi^2}\frac{2 - \Sigma - \Sigma^{-1}}{4 + \Sigma + \Sigma^{-1}}\right) = 0. \tag{36}$$

Three roots exist for (36):

$$\Omega_1^{\text{case-2}} = \hat{\imath}T_* K, \tag{37}$$

$$\Omega_{2,3}^{\text{case-2}} = \frac{\hat{\imath}T_* K}{2} \pm \left(-\frac{T_*^2 K^2}{4} + \frac{6}{\pi^2}\frac{2 - \Sigma - \Sigma^{-1}}{4 + \Sigma + \Sigma^{-1}}\right)^{1/2}. \tag{38}$$

Equations (37) and (38) describe the dispersion of waves for the WE solution at interior nodes. The first root represents a numerical artefact associated with the time differentiation performed to derive the WE. The second and third roots again represent a forward- and a backward-progressing wave respectively. The absolute values of the interior node WE roots are plotted together with the analytical roots against dimensionless wave number for the case $T_* = 0{\cdot}4$ in Figure 14. We note that the WE solution at interior nodes has a monotonic dispersion relationship like the analytical solution. Platzman[30] explained the superior solution properties of the WE-based solution using these dispersion curves by noting that only a physical wave is permitted in the numerical solution. Finally we note that the WE solution is consistent with the analytical solution.

Case 3. Primitive continuity and essential normal flow boundary condition on boundary nodes

We now apply dispersion analysis to boundary nodes by examining the primitive continuity equation on a boundary node in conjunction with a specified homogeneous normal flow

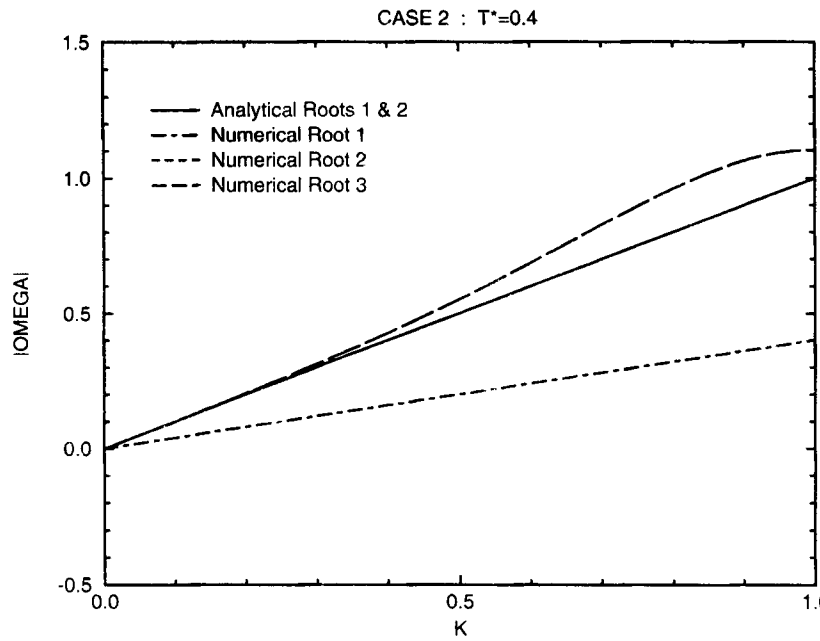

Figure 14. Dispersion curves for Case 2, wave equation and momentum equation on interior nodes

boundary condition equation which replaces the momentum equation at land boundary nodes in the PE-S solution. These discrete equations are written for the left-hand boundary (node 1) in a one-dimensional grid as

$$(\hat{\imath}\omega/6)(2\hat{\zeta}_1 + \hat{\zeta}_2) + (h/2\Delta x)(\hat{u}_2 - \hat{u}_1) = 0, \tag{39}$$

$$\hat{u}_1 h = 0. \tag{40}$$

Substitution of the Fourier solution components (22) and (23) and subsequent rearrangement of these equations lead to the following system of equations in matrix form:

$$\begin{bmatrix} (\hat{\imath}\omega/6)(2+\Sigma) & (h/2\Delta x)(\Sigma - 1) \\ 0 & 1 \end{bmatrix} \begin{bmatrix} Z_0 \\ U_0 \end{bmatrix} = \begin{bmatrix} 0 \\ 0 \end{bmatrix}. \tag{41}$$

For a non-trivial solution the determinant of (41) must be zero. In non-dimensional form this may be expressed as

$$\hat{\imath}\Omega(2 + \Sigma) = 0. \tag{42}$$

Only one root exists for (42):

$$\Omega_1^{\text{case-3}} = 0. \tag{43}$$

This root is plotted in Figure 15 and indicates that infinite aliasing occurs when a primitive continuity equation is paired with an essential normal flow boundary condition at boundary nodes.

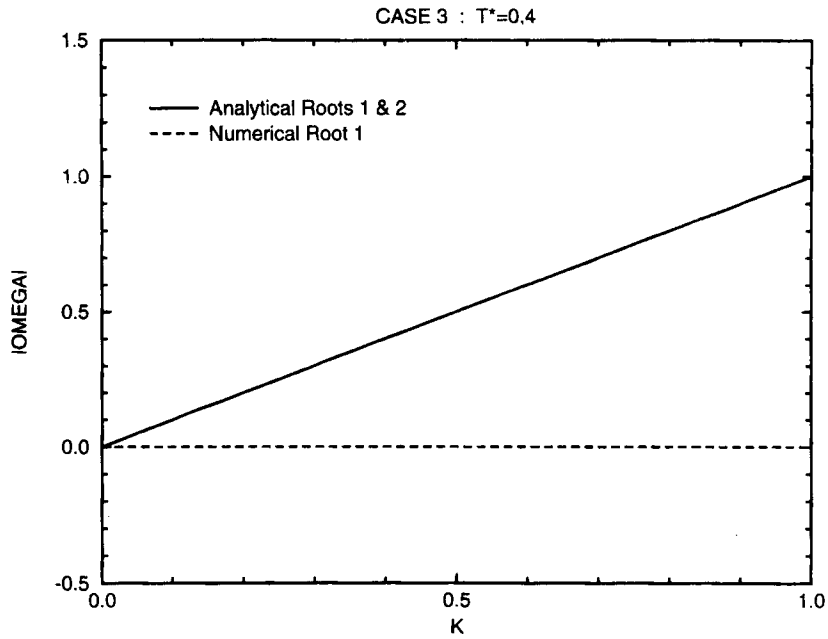

Figure 15. Dispersion curves for Case 3, primitive continuity and essential normal flow boundary condition on boundary nodes

Case 4. Wave equation and essential normal flow boundary condition on boundary nodes

We continue our analysis by examining the wave equation on a boundary node paired with a specified homogeneous normal flow boundary condition equation which replaces the momentum equation at land boundary nodes in the WE-S solution. The pertinent discrete equations are written for the left-hand boundary (node 1) in a one-dimensional grid as

$$(1/6)(-\omega^2 + \hat{\imath}\omega\tau_*)(2\hat{\zeta}_1 + \hat{\zeta}_2) - (hg/\Delta x^2)(\hat{\zeta}_2 - \hat{\zeta}_1) - (\hat{\imath}\omega + \tau_*)(h/\Delta x)\hat{u}_1 = 0, \tag{44}$$

$$\hat{u}_1 h = 0. \tag{45}$$

Fourier analysing these equations by substituting in (22) and (23) and simplifying leads to the following system of equations:

$$\begin{bmatrix} \frac{1}{6}(-\omega^2 + \hat{\imath}\omega\tau_*)(2 + \Sigma) - (hg/\Delta x^2)(\Sigma - 1) & -(\hat{\imath}\omega + \tau_*)(h/\Delta x) \\ 0 & 1 \end{bmatrix} \begin{bmatrix} Z_0 \\ U_0 \end{bmatrix} = \begin{bmatrix} 0 \\ 0 \end{bmatrix}. \tag{46}$$

Setting the determinant of (46) equal to zero leads to the following dispersion equation written in non-dimensional form:

$$\Omega^2 - \hat{\imath}T_* K\Omega + \frac{6}{\pi^2}\frac{\Sigma - 1}{\Sigma + 2} = 0. \tag{47}$$

Equation (47) has two roots:

$$\Omega_{1,2}^{\text{case-4}} = \frac{\hat{\imath}T_* K}{2} \pm \left(-\frac{T_*^2 K^2}{4} - \frac{6}{\pi^2}\frac{\Sigma - 1}{\Sigma + 2} \right)^{1/2}. \tag{48}$$

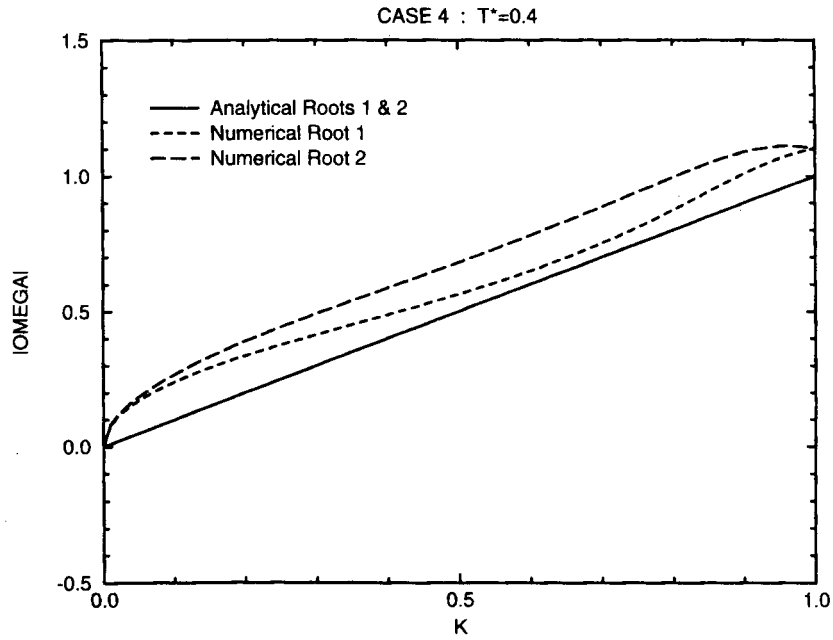

Figure 16. Dispersion curves for Case 4, wave equation and essential normal flow boundary condition on boundary nodes

The absolute values of the dimensionless frequencies given by (48) are plotted against dimensionless wave number for the frictional case $T_* = 0{\cdot}4$ in Figure 16. We note that the dispersion curves associated with the WE paired with a no-normal-flow boundary condition at boundary nodes are non-folded but inconsistent.

Case 5. Elevation boundary condition and momentum equation on boundary nodes

Dispersion analysis is next applied to boundary nodes for which a homogeneous elevation boundary condition is treated as an essential condition, i.e. it replaces the PE or WE, and is paired with a momentum equation at the boundary node. The discrete form of these equations for the left-hand boundary (node 1) is expressed as

$$\hat{\zeta}_1 = 0, \tag{49}$$

$$(\hat{\imath}\omega + \tau_*)(h/6)(2\hat{u}_1 + \hat{u}_2) + (gh/2\Delta x)(\hat{\zeta}_2 - \hat{\zeta}_1) = 0. \tag{50}$$

Equations (49) and (50) are applied at specified elevation boundary nodes for the PE-S, WE-S, PE-E, WE-E and PE-W solutions presented in this paper. Applying Fourier analysis by substituting (22) and (23) into (49) and (50) and simplifying leads to the following system of equations:

$$\begin{bmatrix} 1 & 0 \\ (gh/2\Delta x)(\Sigma - 1) & (\hat{\imath}\omega + \tau_*)(h/6)(2 + \Sigma) \end{bmatrix} \begin{bmatrix} Z_0 \\ U_0 \end{bmatrix} = \begin{bmatrix} 0 \\ 0 \end{bmatrix}. \tag{51}$$

The determinants of (51) must be zero for a non-trivial solution, which leads to the following dispersion equation expressed in non-dimensional form:

$$(\hat{\imath}\Omega + T_* K)(h/6)(2 + \Sigma) = 0. \tag{52}$$

Equation (52) has only one root:

$$\Omega_1^{\text{case-5}} = \hat{\imath} T_* K. \tag{53}$$

This root is in fact identical to the artificial root which arises with the WE solution discrete equations at interior nodes (i.e. Case 2, root $\Omega_1^{\text{case-2}}$). The root is non-folded but inconsistent for cases where $T_* > 0$ as is shown in Figure 17. If $T_* = 0$, equation (53) implies infinite aliasing, but this case does not occur in practice because a frictionless system leads to an unstable solution.

Case 6. Weak form of the primitive continuity equation and momentum equation on boundary nodes

Finally we apply dispersion analysis to boundary nodes which utilize the weak form of the primitive continuity equation paired with the momentum equation. These discrete equations are applied for specified no-normal-flow boundary nodes in the PE-W solution and are expressed at the left-hand boundary (node 1) in a one-dimensional grid as

$$(\hat{\imath}\omega/6)(2\hat{\zeta}_1 + \hat{\zeta}_2) + (h/2\Delta x)(\hat{u}_2 - \hat{u}_1) = 0, \tag{54}$$

$$(\hat{\imath}\omega + \tau_*)(h/6)(2\hat{u}_1 + \hat{u}_2) + (gh/2\Delta x)(\hat{\zeta}_2 - \hat{\zeta}_1) = 0. \tag{55}$$

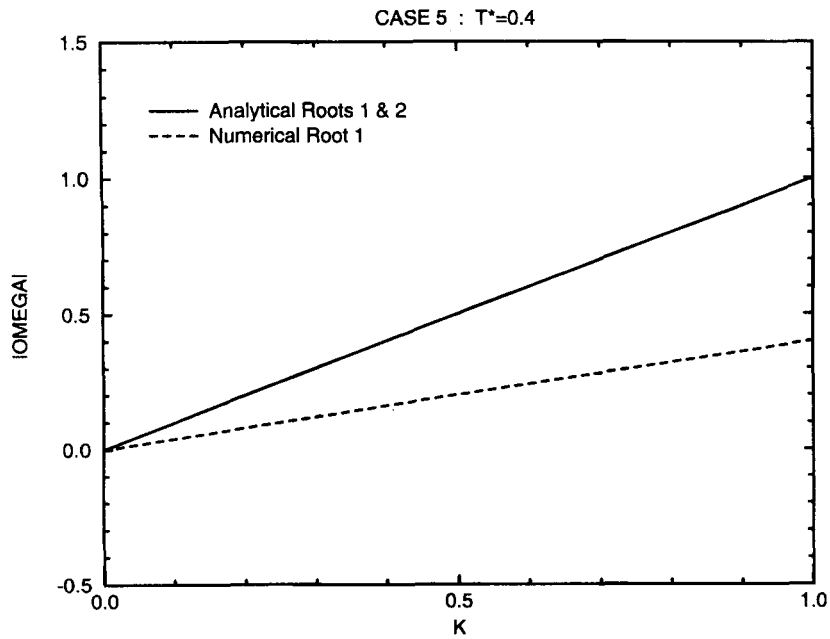

Figure 17. Dispersion curves for Case 5, elevation boundary condition and momentum equation on boundary nodes

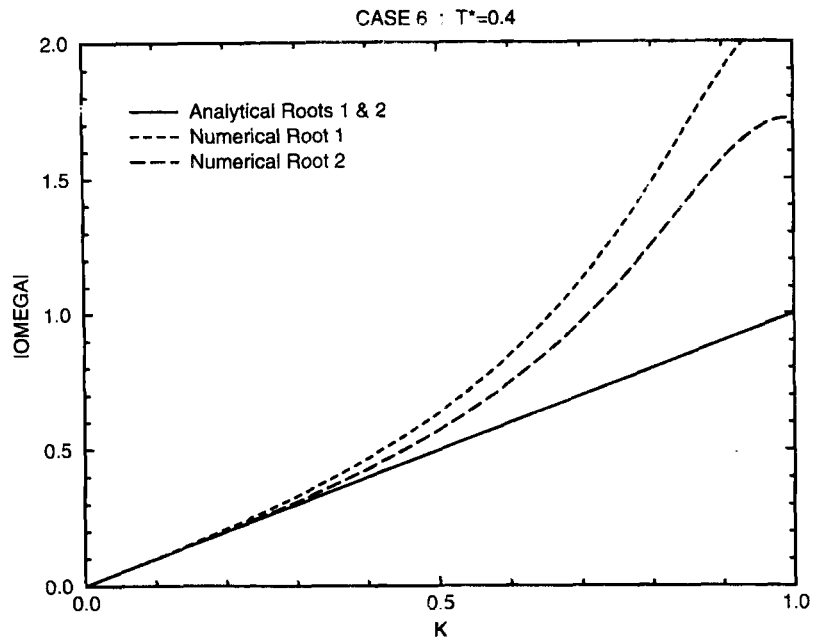

Figure 18. Dispersion curves for Case 6, weak form of primitive continuity equations and momentum equation on boundary nodes

Fourier analysing these equations by substituting in (22) and (23) and simplifying yields the following system of equations:

$$\begin{bmatrix} (\hat{\imath}\omega/6)(2+\Sigma) & (h/2\Delta x)(\Sigma-1) \\ (gh/2\Delta x)(\Sigma-1) & (\hat{\imath}\omega+\tau_*)(h/6)(2+\Sigma) \end{bmatrix} \begin{bmatrix} Z_0 \\ U_0 \end{bmatrix} = \begin{bmatrix} 0 \\ 0 \end{bmatrix}. \tag{56}$$

Setting the determinant of (56) equal to zero leads to the following dispersion equation expressed in non-dimensional form:

$$\Omega^2 - \hat{\imath}T_* K\Omega + \frac{6^2}{4\pi^2}\frac{(\Sigma-1)^2}{(\Sigma+2)^2} = 0. \tag{57}$$

Equation (57) has two roots:

$$\Omega_{1,2}^{\text{case-6}} = \frac{\hat{\imath}T_* K}{2} \pm \left(-\frac{T_*^2 K^2}{4} - \frac{6^2}{4\pi^2}\frac{(\Sigma-1)^2}{(\Sigma+2)^2} \right)^{1/2}. \tag{58}$$

Figure 18 plots the absolute value of these roots for the case $T_* = 0{\cdot}4$ and indicates that the dispersion curves are monotonic and consistent for the case where the weak form of the primitive continuity equation is paired with a momentum equation at no-normal-flow boundary nodes.

DISCUSSION

We have presented a number of solutions to the shallow water equations and examined the characteristics of each solution using numerical experiments and convergence tests. We have also performed dispersion analyses for discrete equation pairs on interior nodes as well as on boundary nodes which are components of the various solution strategies examined in the

numerical experiments. We now re-examine each solution and relate the behaviour seen in the numerical experiments to the various dispersion analyses performed.

The well-known PE-S solution solves the primitive continuity equation in conjunction with the momentum equations. For seaward boundary nodes a standard essential elevation boundary condition is implemented by replacing the continuity equation at the boundary node with the specified elevation value. For land boundary nodes an essential no-normal-flow boundary condition is enforced by replacing the momentum equation at the boundary node with a specified zero-normal-flow condition. The numerical experiments and convergence tests lead to the well-known noisy solutions with numerical short waves persisting regardless of the degree of grid refinement. The results of the dispersion analyses performed for Cases 1, 3 and 5 concur with the numerical experiments performed, namely a folded dispersion curve is associated with a noisy solution. Both PE-S interior nodes (Case 1) as well as PE-S no-normal-flow boundary nodes (Case 3) have folded dispersion relationships allowing the existence of a long physical wave as well as a short near-$2\Delta x$ artificial wave. Although PE-S specified elevation seaward nodes (Case 5) have a monotonic linear dispersion curve, the interior and specified no-normal-flow boundary nodes significantly outnumber the specified elevation seaward nodes and therefore dominate the overall behaviour of the solution.

The highly successful WE-S solution solves the WE in conjunction with the momentum equations. For seaward boundary nodes a standard elevation boundary condition treatment is realized by substituting the specified elevation value for the WE. For land boundary nodes an essential no-normal-flow boundary condition is enforced by replacing the momentum equation at the boundary nodes with a specified zero-normal-flow equation. The numerical simulations presented confirm that the WE-S solutions are excellent and that no spurious modes are generated regardless of the discretization used. The results of the dispersion analyses for Cases 2, 4 and 5 corroborate the observed numerical behaviour. The dispersion curves for all WE-S discrete equations including interior nodes (Case 2), no-normal-flow boundary nodes (Case 4) and specified elevation seaward boundary nodes (Case 5) are monotonic. Thus only one physical long wave is allowed in the solution.

The PE-E solution solves the primitive continuity equation in conjunction with the momentum equations. All boundary nodes have specified essential elevation boundary conditions which replace the continuity equation at the boundary nodes. Interestingly, the PE-E elevation solutions obtained in our numerical experiments are noise-free and show excellent agreement with the analytical solution. Velocity solutions were good in the interior of the domain but did not reduce to zero normal flow on land boundaries, allowing some leakage near the interior boundary of the domain. Our dispersion analyses indicate that while PE-E interior nodes (Case 1) have a folded dispersion behaviour, the specified elevation boundary nodes (Case 5) have an associated linear monotonic dispersion curve. Based on the results of the numerical experiments, we infer that the influence of the boundary nodes with their monotonic dispersion behaviour is sufficient to suppress the spurious mode character of the interior nodes, thus leading to an overall solution essentially free of noise.

The WE-E solution studied solves the WE in conjunction with the momentum equations with all boundary nodes having specified essential elevation boundary conditions which replace the WE at the boundary nodes. The numerical experiments indicate that the WE-E solution continues to produce smooth and accurate solutions. We do note that the WE-E solution exhibits the same mass leakage problem as the PE-E solution. The results of dispersion analyses again match the numerical experiments in that both interior WE-E nodes (Case 2) as well as specified elevation boundary nodes (Case 5) have monotonic dispersion relationships.

Finally, the PE-W algorithm solves a weak form of the primitive continuity equation in conjunction with the momentum equations. For seaward boundary nodes a standard essential

elevation boundary condition is implemented by replacing the continuity equation at the boundary node with the specified elevation value. For land boundary nodes a natural no-normal-flow boundary condition is enforced by computing the boundary integral in the weak form of the continuity equation. No momentum equations are discarded at land boundary nodes. While the discrete equation pairs are the same as for the PE-S solution for interior and seaward boundary nodes, they are significantly different for the land boundary nodes. Again the numerical experiments indicate that the PE-W solutions do not exhibit the characteristic noisy behaviour of the PE-S solutions. Both the elevation and velocity solutions are very good with the exception of the same mass imbalance problem at the inner land boundary which appeared in the PE-E and WE-E solutions. Note that the PE-W solution converges very nicely and that no spurious modes appear even for the finest grids. Dispersion analyses can be used to explain why the PE-W solution does not exhibit the same behaviour as the PE-S solution. While the PE-W interior nodes have an associated folded dispersion curve (Case 1), both PE-W specified elevation seaward nodes (Case 5) and PE-W no-normal-flow boundary nodes (Case 6) have associated monotonic dispersion curves. Again based on the results of the numerical experiments, we infer that the influence of the boundary nodes with their monotonic dispersion behaviour is sufficient to suppress the spurious mode character of the interior nodes. We note that it is the dispersion character of the entire system of nodes that is important and that the dispersion behaviour of the system need only be sufficiently elevated at the high-wave-number portion of the spectrum to avoid dual wave numbers for the pertinent forcing and response frequencies.[43]

CONCLUSIONS

The numerical experiments presented in this paper indicate that while WE solutions to the linearized harmonic shallow water equations are insensitive to boundary conditions, PE solutions are significantly affected by boundary condition implementation. The WE-S and WE-E solutions always lead to excellent noise-free solutions. The PE-S solutions are very poor, being contaminated with high-wave-number noise while the PE-E and PE-W solutions are very good and generally free of numerical noise. The presence of noise appears to be insensitive to the degree of grid refinement and to network irregularities in all solutions with the exception of the PE-S solution.

Dispersion analyses of both interior and boundary node equation pairs offer a satisfactory explanation for the observed behaviour. The WE solutions exhibit a monotonic dispersion behaviour for interior as well as boundary nodes for both elevation and no-normal-flow boundary conditions. On the other hand, the PE solutions always have folded dispersion curves for interior nodes but may or may not have similar curves for boundary nodes. In particular, PE solutions have folded dispersion curves at boundary nodes when essential no-normal-flow boundary conditions are used but have monotonic curves at boundary nodes when essential elevation or natural no-normal-flow boundary conditions are used. In the PE-E and PE-W solutions the monotonic dispersion behaviour of the boundary nodes is sufficient to suppress the folded dispersion behaviour of the interior nodes; this results in an overall dispersion behaviour of the system which is sufficiently elevated at the high-wave-number portion of the spectrum to avoid dual wave numbers for the frequency range of interest.

In closing, we note that our study has focused on the linear harmonic shallow water equations applied to highly idealized cases (i.e. the numerical experiments were applied to a linear problem with a regular two-dimensional domain with regular varying bathymetry and idealized boundary conditions on a regular boundary, and the dispersion analyses were applied to a one-dimensional problem with constant bathymetry). Even though the experiments in this paper

indicate that the quarter-annulus test problem solved with the PE-E and PE-W solutions was nearly as successful and the WE-S and WE-E solutions, our experience indicates that field applications using the PE-W-based solutions are still not as robust or noise-free as WE-S solutions.[26–28,44,45] This is most likely a result of the PE-W solution being dependent on the characteristics of the boundary nodes compensating for the poor behaviour of the interior nodes. The WE solutions on the other hand have excellent numerical properties at both interior and boundary nodes. Therefore, although the present study has provided additional insight to the behaviour of both PE and WE solutions with various boundary condition implementations, we strongly recommend that the WE solution strategy be used in practical applications.

ACKNOWLEDGEMENT

This research was funded in part by the U.S. Army Waterways Experiment Station under contract number DACW 39-90-K-0021.

REFERENCES

1. J. D. Wang and J. J. Connor, 'Mathematical modeling of near coastal circulation', *R. M. Parsons Laboratory Rep. 200*, Massachusetts Institute of Technology, Cambridge, MA, 1975.
2. C. Taylor and J. Davis, 'Tidal and long wave propagation—a finite element approach', *Comput. Fluids*, **3**, 125–148 (1975).
3. C. A. Brebbia and P. Partridge, 'Finite element models for circulation studies', *Mathematical Models for Environmental Problems: Int. Conf. Proc.*, Southhampton, 1975.
4. M. Kawahara, N. Takeuchi and T. Yoshida, 'Two step explicit finite element method for tsunami wave propagation analysis', *Int. j. numer. methods eng.*, **12**, 331–351 (1978).
5. J. J. Connor and J. D. Wang, 'Finite element modeling of hydrodynamic circulation', in C. A. Brebbia and J. J. Connor (eds), *Numerical Methods in Fluid Dynamics*, Pentech, London, 1974.
6. R. G. Kelley Jr. and R. T. Williams, 'A finite element prediction model with variable element sizes', *Rep. NPS-63WU76101*, Naval Postgraduate School, Monterey, CA, 1976.
7. F. D. Malone and J. T. Kuo, 'Semi-implicit finite element methods applied to the shallow water equations', *J. Geophys. Res.*, **86**, 4029–4040 (1981).
8. P. M. Gresho and R. L. Lee, 'Don't suppress the wiggles—they're telling you something', *Comput. Fluids*, **9**, 223–253 (1981).
9. W. G. Gray, 'Some inadequacies of finite element models as simulators of two-dimensional circulation', *Adv. Water Resources*, **5**, 171–177 (1982).
10. D. R. Lynch, 'Progress in hydrodynamic modeling, review of U.S. contributions, 1979–1982', *Rev. Geophys. Space Phys.*, **21**, 741–754 (1983).
11. M. B. Abbot, 'Numerical modeling for coastal and ocean engineering', in J. Herbich (ed.), *Handbook of Coastal and Ocean Engineering*, Gulf, 1989.
12. J. J. Westerink and W. G. Gray, 'Progress in surface water modeling', *Rev. Geophys.*, **29**, 210–217 (1991).
13. R. A. Walters and G. F. Carey, 'Analysis of spurious oscillation modes for the shallow water and Navier–Stokes equations', *Comput. Fluids*, **11**, 51–68 (1983).
14. R. A. Walters, 'Numerically induced oscillations in finite element approximations to the shallow water equations', *Int. j. numer. methods fluids*, **3**, 591–604 (1983).
15. R. A. Walters, 'Finite element solution methods for circulation in estuaries', in J. P. Laible *et al.* (eds), *Finite Elements in Water Resources: Proc. 5th Int. Conf.*, Burlington, VT, 1984.
16. D. R. Lynch and W. G. Gray, 'A wave equation model for finite element tidal computations', *Comput. Fluids*, **7**, 207–228 (1979).
17. I. P. E. Kinnmark and W. G. Gray, 'An implicit wave equation model for the shallow water equations', *in J. P. Laible et al. (eds), Finite Elements in Water Resources: Proc. 5th Int. Conf.*, Burlington, VT, 1984.
18. D. R. Lynch, 'Comparison of spectral and time-stepping approaches for finite element modeling of tidal circulation', *Oceans 81 Conf. Rec.*, Boston, MA, *IEEE Pub. 81CH1685-7*, 1981.
19. M. G. G. Foreman, 'A comparison of tidal models for the southwest coast of Vancouver Island', *Proc. 7th Int. Conf. on Computational Methods in Water Resources*, Elsevier Amsterdam, 1988.
20. D. R. Lynch, F. E. Werner, A. Cantos-Figuerola and G. Parilla, 'Finite element modeling of reduced-gravity flow in the Alboran Sea: sensitivity studies', *Seminario Sobre Oceanografia Fisica del Estrecho de Gibraltar*, Madrid, 1988, pp. 283–295.

21. R. A. Walters, 'A finite element model for tides and currents with field applications', *Commun. Appl. Numer. Methods*, **4**, 401–411 (1988).
22. W. G. Gray, 'A finite element study of tidal flow data for the North Sea and English Channel', *Adv. Water Resources*, **12**, 143–154 (1989).
23. R. A. Walters and F. E. Werner, 'A comparison of two finite element models of tidal hydrodynamics using a North Sea data set', *Adv. Water Resources*, **12**, 184–193 (1989).
24. F. E. Werner and D. R. Lynch, 'Harmonic structure of English Channel/Southern Bight tides from a wave equation simulation', *Adv. Water Resources*, **12**, 121–142 (1989).
25. D. R. Lynch and F. E. Werner, 'Three-dimensional hydrodynamics on finite elements. Part II: Nonlinear time-stepping model', *Int. j. numer. methods fluids*, **12**, 507–533 (1991).
26. J. J. Westerink, R. A. Luettich, A. M. Baptista, N. W. Scheffner and P. Farrar, 'Tide and storm surge predictions using a finite element model', *J. Hydraul. Eng.*, **118**, 1373–1390 (1992).
27. J. J. Westerink, R. A. Luettich and J. C. Muccino, 'Modeling tides in the western North Atlantic using unstructured graded grids', *Tellus*, in press.
28. C. A. Blain, J. J. Westerink and R. A. Luettich, 'The influence of domain size on the response characteristics of a hurricane storm surge model', *J Geophys. Res.*, to appear.
29. C. LeProvost and A. Poncet, 'Finite element method for spectral modeling of tides', *Int. j. numer methods eng.*, **12**, 853–871 (1978).
30. G. W. Platzman, 'Some response characteristics of finite element tidal models', *J. Comput. Phys.*, **40**, 36–63 (1981).
31. W. G. Gray and D. R. Lynch, 'Time-stepping schemes for finite element tidal model computations', *Adv. Water Resources*, **1**, 83–95 (1977).
32. M. G. G. Foreman, 'An analysis of two-step time discretizations in the solution of the linearized shallow water equations', *J. Comput. Phys.*, **51**, 454–483 (1983).
33. M. G. G. Foreman, 'An analysis of the "wave equation" model for finite element tidal computations', *J. Comput. Phys.*, **52**, 290–312 (1983).
34. R. L. Sani, P. M. Gresho, R. L. Lee and D. F. Griffiths, 'The cause and cure (?) of the spurious pressures generated by certain FEM solutions of the incompressible Navier–Stokes equations: Part 1', *Int. j numer. methods fluids*, **1**, 17–43 (1981).
35. R. L. Sani, P. M. Gresho, R. L. Lee, D. F. Griffiths and M. Engleman, 'The cause and cure (!) of the spurious pressures generated by certain FEM solutions of the incompressible Navier–Stokes equations: Part 2', *Int. j. numer. methods fluids*, **1**, 171–204 (1981).
36. T. J. R. Hughes and A. N. Brooks, 'A multidimensional upwind scheme with no crosswind diffusion', in T. J. R. Hughes (ed.), *Finite Element Methods for Convection Dominated Flows*, ASME, New York, 1979.
37. G. K. Verboom and A. Slob, 'Weakly-reflective boundary conditions for two-dimensional shallow water flow problems', in J. P. Laible *et al.* (eds), *Finite Elements in Water Resources: Proc. 5th Int. Conf.*, Burlington, VT, 1984.
38. D. R. Lynch, 'Mass balance in shallow water simulations', *Commun. Appl. Numer Methods*, **1**, 153–159 (1985).
39. M. G. G. Foreman, 'An accuracy analysis of boundary conditions for the forced shallow water equations', *J. Comput. Phys.*, **64**, 334–367 (1986).
40. J. Drolet and W. G. Gray, 'On the well posedness of some wave formulations of the shallow water equations', *Adv. Water Resources*, **11**, 84–91 (1988).
41. D. R. Lynch and W. G. Gray, 'Analytical solutions for computer flow model testing, *ASCE J. Hydraul. Div.*, **104**, 1409–1428 (1978).
42. W. G. Gray, 'On normal flow boundary conditions in finite element codes for two-dimensional shallow water flow', *Int. j. numer. methods fluids*, **4**, 99–104 (1984).
43. R. L. Kolar, J. J. Westerink, M. E. Cantekin and C. A. Blain, 'Aspects of nonlinear simulations using shallow water models based on the wave continuity equation', *Comput. Fluids*, **23**, 523–538 (1994).
44. A. M. Baptista, J. J. Westerink and P. J. Turner, 'Tides in the English Channel and southern North Sea. A frequency domain analysis using model TEA-NL', *Adv. Water Resources*, **12**, 166–183 (1989).
45. J. J. Westerink, K. D. Stolzenbach and J. J. Connor, 'General spectral computations of the nonlinear shallow water tidal interactions within the Bight of Abaco', *J. Phys. Oceanogr.*, **19**, 1348–1371 (1989).